In-situ estimation of subsurface hydro-geomechanical properties using the groundwater response to Earth and atmospheric tides

Timothy C. McMillan[1,2], Martin S. Andersen[1], Wendy A. Timms[3], Gabriel C. Rau[4]

[1]School of Civil and Environmental Engineering, The University of New South Wales, Sydney, Australia
[2]School of Mineral and Energy Resource Engineering, The University of New South Wales, Sydney, Australia
[3]School of Engineering, Deakin University, Waurn Ponds, Australia
[4]Institute of Applied Geosciences (AGW), Karlsruhe Institute of Technology (KIT), Karlsruhe, Germany

Key Points:

- A new in-situ method to estimate subsurface hydraulic and poroelastic parameters for unconsolidated and consolidated systems
- For consolidated systems, the approach only requires one assumption of the grain compressibility
- Application to data from four field sites gives appropriate results and reveals new insights

Corresponding author: Gabriel C. Rau, gabriel.rau@kit.edu

Abstract

Subsurface hydro-geomechanical properties crucially underpin the management of Earth's resources, yet they are predominantly measured on core-samples in the laboratory while little is known about the representativeness of in-situ conditions. The impact of Earth and atmospheric tides on borehole water levels are ubiquitous and can be used to characterize the subsurface. We illustrate that disentangling the groundwater response to Earth and atmospheric tidal forces in conjunction with hydraulic and linear poroelastic theories leads to a complete determination of the whole parameter space for unconsolidated systems. Further, the characterization of consolidated systems is possible when using literature estimates of the grain compressibility. While previous field investigations have assumed a Poisson's ratio, our new approach allows for its estimation under in-situ conditions. We apply this method to water level and barometric pressure records from four field sites with different hydrogeology. Our results reveal the anisotropic response to strain, which is expected for a heterogeneous lithological profile. Estimated hydro-geomechanical properties (specific storage, hydraulic conductivity, porosity, shear, Young's and bulk moduli, Skempton's and Biot-Willis coefficients and undrained/drained Poisson's ratios) are comparable to values reported in the literature, except for consistently negative drained Poisson's ratios which are surprising. Closer analysis reveals that this can be explained by the fact that in-situ conditions differ from typical laboratory core tests. Our new approach can be used to passively, and therefore cost-effectively, estimate subsurface hydro-geomechanical properties representative of in-situ conditions. Our method could be used to improve understanding of the relationship between geological and geomechanical subsurface heterogeneity.

Plain Language Summary

Earth resource exploitation requires knowledge of the subsurface physical properties. This work develops a new method to estimate hydraulic and geomechanical subsurface properties in-situ using standard groundwater and atmospheric pressure records. The approach is illustrated through application to four field sites with different hydrogeological settings. The estimated results are all similar to standard test results except for the Poisson ratio which we attribute to the investigated scale and conditions. Our new approach can be used to investigate a subsurface system using established groundwater monitoring practice.

1 Introduction

A perpetual challenge for subsurface water, mineral resource or geotechnical projects is a proper characterization of the physical properties that may have bearings on the rate of resource extraction, operation, safety and environmental impact of the project. The main reason for this challenge is the subsurface's heterogeneous nature and that the sampling density necessary to describe it may be prohibitively expensive (e.g. by drilling and testing of core). This issue is further exacerbated by the difficulty in approximating in-situ environments in a laboratory for both scale and subsurface pressures (Hoek & Diederichs, 2006; Cundall et al., 2008; Bouzalakos et al., 2016). These difficulties may be abated by the in-situ characterization of hydro-geomechanical properties of the subsurface (Villeneuve et al., 2018). Here, the in-situ pressure, stress conditions, and the scaling and inclusion of heterogeneities can achieve a more representative estimate than possible in a laboratory.

The utilization of Earth and atmospheric tides (EAT) has been shown to be capable of estimating hydrogeomechanical properties of the subsurface (Hsieh et al., 1987; Rojstaczer & Agnew, 1989; S. Zhang et al., 2019). Further, with the assumption of key variables, previous authors have also been able to extend the use of EAT to estimate subsurface geomechanical properties (Bredehoeft, 1967; Beavan et al., 1991; Cutillo & Bredehoeft, 2011). However, the application of tidal subsurface analysis (TSA) techniques remains underutilized.

Earth and atmospheric tides (EAT) are natural phenomena that occur throughout the Earth's crust, which have been measured and analyzed in the subsurface since the mid-20^{th} century (McMillan et al., 2019). Traditionally this these techniques have been focused on either Earth tides (Bredehoeft, 1967; Hsieh et al., 1987; Cutillo & Bredehoeft, 2011; S. Zhang et al., 2019; Burbey, 2010), barometric pressure (Clark, 1967; Cutillo & Bredehoeft, 2011) or atmospheric tide loading (Acworth et al., 2016; McMillan et al., 2019; Rau et al., 2020) of the confined subsurface. Bredehoeft (1967) first proposed that once specific storage is calculated from the groundwater response to Earth tides, an aquifer porosity and compressibility can be determined from the formation pressure response to a uniformly distributed surface load such as caused by barometric pressure changes (Narasimhan et al., 1984; Rojstaczer, 1988; Rojstaczer & Riley, 1990; Ritzi et al., 1991; Burbey et al., 2012). This concept has been reiterated in the literature but,

to the best of our knowledge, never solved without the use of either an assumed Poisson's ratio or bulk modulus (Cutillo & Bredehoeft, 2011) due to difficulties in attributing the superimposed EAT effects to their appropriate drivers. Recent work estimating amplitudes and phases using *harmonic least squares* (HALS) and synthetically predicted ETs has demonstrated that separating tidal components of very similar frequencies is now possible (Rau et al., 2020). This has opened opportunities to revisit existing methods to create a new integrated approach.

In this paper, the theory of the groundwater response to Earth and atmospheric tides is combined, thereby providing a new methodology for the estimation of the primary (storage, hydraulic conductivity, poroelastic) subsurface hydrogeomechanical properties. This newly introduced method improves upon the work of Cutillo and Bredehoeft (2011), as it quantitatively disentangles the groundwater response to Earth and atmospheric tides within the frequency domain, allowing separate and objective estimation of properties from each driver before combining the strain responses. Here, the hydraulic and linear poroelastic works of Hsieh et al. (1987), Rojstaczer and Agnew (1989), Beavan et al. (1991) and Rau et al. (2020) are integrated and combined, leading to a complete determination of the parameter space for unconsolidated systems. Further, the characterization of consolidated systems is possible when using literature estimates of the grain compressibility (van der Kamp & Gale, 1983; Green & Wang, 1990). Finally, the new methodology is applied to groundwater and atmospheric pressure records in five boreholes from four sites to estimate hydrogeological and geomechanical properties of various consolidated and unconsolidated stratigraphies.

2 Theoretical background

2.1 Extracting tidal components

Atmospheric heating and the gravitational pull of celestial bodies (e.g., Sun or Moon) exert a loading of the Earth's crust (Agnew, 2010). The gravity variations and loading exerted by the movement of these celestial bodies (i.e., the Moon and Sun), as shown in Table 1, cause stress and strain responses in the Earth's crust. This causes a subsurface strain signal that is composed of numerous superimposed signals of various frequencies and amplitudes. For undrained conditions (pressurized) of either confined or semi-

Tidal component (Darwinian name)	Frequency (*cpd*)	Tidal potential ($m^2\,s^{-2}$)	Tidal gravity variation ($m\,s^{-2}$)	Tidal dilatation / areal strain (-)	Description	Attribution
M_2	1.932274	42.060943	$6.477 \cdot 10^{-5}$	$2.625 \cdot 10^{-7}$	Principal lunar semi-diurnal	Earth
S_2	2.000000	19.309855	$2.973 \cdot 10^{-5}$	$1.205 \cdot 10^{-7}$	Principal solar semi-diurnal	Atmosphere/Earth

Table 1. Table of M_2 and S_2 tidal components, tidal potential, gravity and dilatation using tidal predictions (this does not include local variations). Extracted from Agnew (2010) and McMillan et al. (2019).

confined aquifers, this strain manifests as a groundwater pore pressure fluctuation (McMillan et al., 2019). An illustration of these processes is shown in Figure 1.

Three variables are required to calculate subsurface properties using specific harmonic components (McMillan et al., 2019): (1) a computed dilatation strain due to Earth tides (denoted by the superscript ET); (2) measured barometric pressure (denoted by the superscript AT); and (3) measured groundwater heads (denoted by the superscript GW). First, a moving average spanning across a time period of 3 days is applied. This acts like a high-pass filter which discards longer period signals, such as those originating from pressure systems moving across a field site, rainfall, recharge or pumping responses. Then, the tidally induced frequency components are extracted by using the Fast Fourier Transform (De Araujo et al., 2012; Acworth et al., 2016) or amplitude and phase estimates using *harmonic least-squares* (HALS) (Hsieh et al., 1987; Xue et al., 2016; Rau et al., 2020). The results are complex numbers at discrete frequencies ($\hat{z}_{(f)}$, e.g. $\hat{z}_{M_2}$) for which amplitudes and phases can be calculated using the real and imaginary parts.

2.2 Earth tide influences on well water levels

2.2.1 Subsurface strain response to gravity changes

Rojstaczer and Agnew (1989) argued that for Earth tides horizontal areal strain is a sufficient approximation for depths of up to thousands of kilometers. This approximation is sufficient for application to groundwater resources as they are generally much shallower. The strain is often referred to as dilatation which is the total increase in vol-

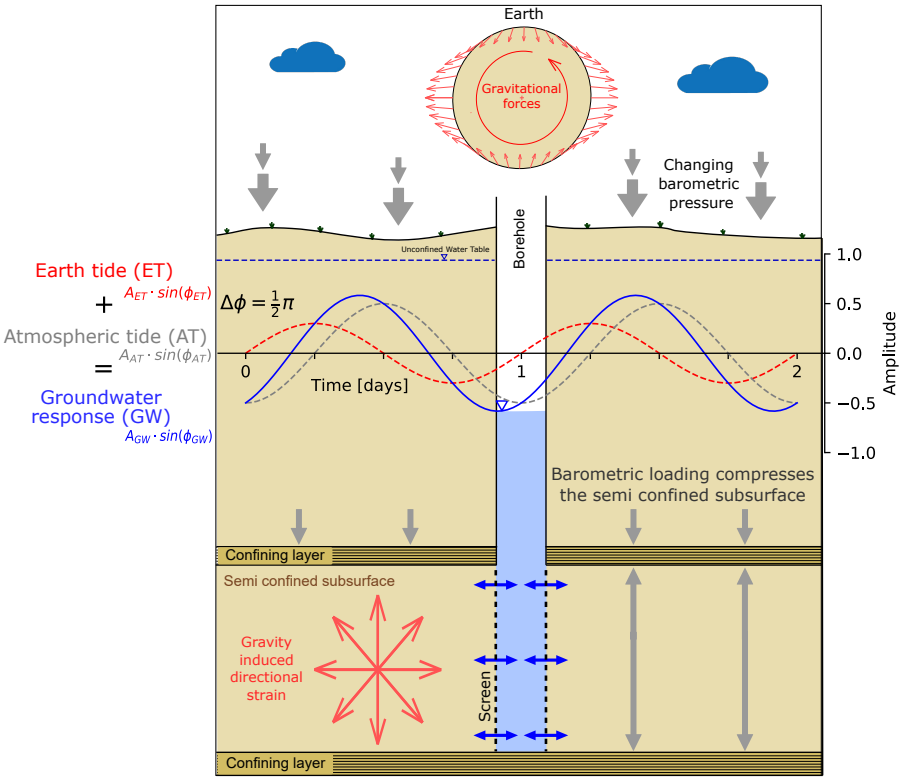

Figure 1. Representation of groundwater pressure head measured in a well penetrating a confined aquifer with a relatively rigid matrix subjected to ET (red) and AT (gray) adapted from (McMillan et al., 2019). The result of these two effects can be expressed as a function of harmonic addition within the groundwater level. Here, the gravity-induced directional strain and vertical barometric loading/unloading combine to force water into and out of the well.

ume of the material due to forcing by the Earth tides (in this case the tidal pull). In porous media, assuming incompressible grains, this dilatation is manifesting as an opening of the total pore space, decreasing the water pressure within the material (Agnew, 2010). In this paper the term 'dilatation' is used broadly for both the dilation and compression due to the cyclical forcing of the tides, coherent with its previous literature use (Xue et al., 2016; Allègre et al., 2016). The distortions by dilatation can be estimated through the planar strain concept known as tidal dilatation (Schulze et al., 2000; Fuentes-Arreazola et al., 2018). Tidal dilatation can be defined as

$$e^t = \frac{V}{g} \cdot \frac{e^v - 3e^h}{R} \tag{1}$$

where e^t is the tidal dilatation strain (-), in this instance at the M_2 frequency, g is acceleration due to gravity ($\approx 9.81 m/s^2$), e^v is vertical displacement (-), e^h is horizontal displacement (-) (Agnew, 2010), R the average radius of the Earth (m) adjusted for any significant elevation and V is the tidal potential as defined in Table 1. The term ($e^v - 3e^h$) may also be approximated by Love-Shida numbers where e^v can be replaced by $\frac{L}{S}h$ with an assumed value of 0.6032 and e^h may be replaced with $\frac{L}{S}l$ with an assumed value of 0.0839 (Agnew, 2010; Cutillo & Bredehoeft, 2011). Calculated strain is generally used for analyzing the groundwater response to Earth tide forces E. Roeloffs (1996); Xue et al. (2016); Allègre et al. (2016); McMillan et al. (2019). As such, the terms e^v and e^h can be directly calculated from software that generates theoretical Earth tides or tidal dilatation strains, for example using *ETERNA* (Wenzel, 1996), *TSoft* (Van Camp & Vauterin, 2005), or as was done for this paper *PyGTide* (Rau, 2018).

The first approach using ET to estimate specific storage, used the potential for water movement from the tides to the corresponding water movement in a monitoring well in a confined aquifer for undrained conditions. An assumed incompressible grain specific storage (S_s) was defined by Bredehoeft (1967) as

$$S_s = -\left[\left(\frac{1-2v}{1-v}\right)\left(\frac{2\frac{L}{S}h - 6\frac{L}{S}l}{R \cdot g}\right)\right]\frac{\Delta A_{M_2}^{ETp}}{\Delta h}, \tag{2}$$

where $\Delta A_{M_2}^{ETp}$ is the change in the tidal potential to the corresponding change in hydraulic head Δh and v is an assumed Poisson's ratio. Here, the tidal dilatation has been included in its definition, Equation 1. This method (Equation 2) by Bredehoeft (1967) was used in Cutillo and Bredehoeft (2011) and is advantageous as it does not require the separation of individual tidal components or knowledge of the well's dimensions. Progressive improvements in the precision and duration of gravity measurement methods have

since allowed for more accurate decomposition and cataloging of the various tidal components (Agnew, 2010). These established catalogs of precise frequencies provide the basis for component separation using harmonic filtering techniques. The full separation of ET and AT at one frequency allows their individual and combined use towards better in-situ hydrogeomechanical characterization (Rau et al., 2020).

2.2.2 Well water level response to harmonically forced pore pressure

In this paper, we will be using HALS, focusing on the ET component at the frequency of 1.932274 *cpd* (denoted by a subscript of its Darwin name M_2) and the combined ET and AT component at the frequency of 2 *cpd* (denoted by a subscript of its Darwin name S_2), described in Table 1. These two components have the strongest tidal potential for ET and AT respectively, however, other frequency components can also be used (Hsieh et al., 1988; Merritt, 2004; Cutillo & Bredehoeft, 2011).

The relative amplitude response of the groundwater, as measured in a borehole in relation to the tidal dilatation strain can be expressed as (Hsieh et al., 1987; Xue et al., 2016; Allègre et al., 2016)

$$A^e_{M_2} = \left| \frac{\hat{z}^{GW}_{M_2}}{\hat{z}^{ETe}_{M_2}} \right| = \frac{A^{GW}_{M_2}}{A^{ETe}_{M_2}}, \tag{3}$$

where $\hat{z}^{GW}_{M_2}$ and $\hat{z}^{ETe}_{M_2}$ are the complex frequency component of the groundwater pressure head and tidal dilatation strain, respectively; $A^{GW}_{M_2}$ is the amplitude of the groundwater pressure head fluctuation and $A^{ETe}_{M_2}$ is the amplitude of the tidal dilatation strain fluctuation, all at the frequency of the M_2 tidal component. Note that $A^e_{M_2}$ is also referred to as areal strain sensitivity (Hsieh et al., 1987).

It is important to note the difference presented in Equation 3 from Xue et al. (2016) with the original dimensionless amplitude response calculated by Hsieh et al. (1987) as

$$A_{M_2} = \left| \frac{\hat{z}^{GW}_{M_2}}{\hat{z}^{p}_{M_2}} \right| = A^e_{M_2} S_s, \tag{4}$$

where $\hat{z}^{p}_{M_2}$ is the complex aquifer pore pressure response (superscript p reflects pore). Here, the denominator term has changed from the complex amplitude of the pressure fluctuation with the tidal dilatation, effectively incorporating Equation 2. This key difference allows for the addition of the term S_s within the amplitude response equations due to the sensitivity of storage to the amplitude response for post- and pre-strain responses described in Sections 2.2.3 and 2.2.4. Equation 4 is dimensionless with values $0 \leq A_{M_2} \leq 1$.

The phase shift (or difference) is defined as the strain response observed as the complex groundwater pressure head (water level) fluctuation, minus the phase of the complex tidal dilation (tidal forcing) stress, defined as

$$\Delta\phi_{M_2} = \arg\left(\frac{\hat{z}_{M_2}^{GW}}{\hat{z}_{M_2}^{ETe}}\right) = \phi_{M_2}^{GW} - \phi_{M_2}^{ETe}, \tag{5}$$

where $\phi_{M_2}^{GW}$ is the phase angle expressed in groundwater and $\phi_{M_2}^{ETe}$ is the phase angle of the theoretical Earth tide component, in this case at the frequency of the M_2. A negative phase shift is expressed where the groundwater lags behind the induced strain (water level response lags behind the pressure head disturbance (Hsieh et al., 1987)), whereas a positive phase shift indicates the groundwater response is leading the strain response.

It should be noted that in this method development, a homogeneous, isotropic aquifer of infinite lateral extent is assumed for all derivations (Hsieh et al., 1987). All derived hydro-geomechanical variables are treated as bulk properties (averaged over a distinct but unknown volume), representative of the EAT area of influence around the monitoring wells screened interval, including effects from geological heterogeneities and the well construction, such as the inclusion of a gravel pack. The exact nature and dimensions of the volume of influence (i.e. the volume of sub-surface around the well being 'sampled') is currently unresolved. It is commonly assumed that the ET amplitude response is negligibly influenced by fluid flow when confined (Xue et al., 2016); instead, it is predominantly controlled by the storage. This is used as a justification to modify the first hydraulic diffusivity term in the amplitude response equations to $1/Ss$ when including the Earth tide strain estimation (Equations 6 and 14), i.e. the tidal dilatation (Hsieh et al., 1987; H. F. Wang, 2000; Xue et al., 2016).

2.2.3 Post-strain water level response

Positive and negative phase shifts are either leading (pre-strain) or lagging (post-strain), respectively, in relation to the strain response expressed by the water level in a well to formation tidal forcing. Hsieh et al. (1987) provided an analytical solution for the confined groundwater flow equation with harmonic forcing to describe the relationship between aquifer pore pressure and well water level. Their model is formulated in terms of amplitude ratio and phase shift, thereby allowing for the solution of two properties, transmissivity and storativity from the amplitude and phase response. This model works by exploiting the lack of sensitivity to storage within the phase shift equation and

iterates to fit for both transmissivity and storage (See Figure 3) (Rau et al., 2020). The post-strain (negative phase) model is defined by Hsieh et al. (1988) as

$$A^e_{M_2} = \frac{1}{S_s}(E^2 + F^2)^{-\frac{1}{2}} \tag{6}$$

and

$$\Delta\phi_{M_2} = -\tan^{-1}\left(\frac{F}{E}\right) \tag{7}$$

where

$$E = 1 - \frac{\omega r_c^2}{2T}[\Psi Ker(\alpha_w) + \psi Kei(\alpha_w)] \tag{8}$$

and

$$F = \frac{\omega r_c^2}{2T}[\psi Ker(\alpha_w) - \Psi Kei(\alpha_w)] \tag{9}$$

and

$$\Psi = \frac{-[Ker_1(\alpha_w) - Kei_1(\alpha_w)]}{2^{\frac{1}{2}}\alpha_w[Ker_1^2(\alpha_w) + Kei_1^2(\alpha_w)} \tag{10}$$

and

$$\psi = \frac{-[Ker_1(\alpha_w) + Kei_1(\alpha_w)]}{2^{\frac{1}{2}}\alpha_w[Ker_1^2(\alpha_w) + Kei_1^2(\alpha_w)]} \tag{11}$$

where

$$\alpha_w = r_w\sqrt{\frac{\omega S}{T}} = r_w\sqrt{\frac{\omega}{D_h}}. \tag{12}$$

The storativity S, can be related to specific storage as

$$S = S_s b \tag{13}$$

where b is the aquifer thickness, here equivalent to the vertical screen length when the aquifer thickness is unknown, r_w is the internal radius of the well screen (accounts for well storage), r_c is the radius of the casing. Ker and Kei are Kelvin functions of zero order, and Ker_1 and Kei_1 are Kelvin functions of the first order.

2.2.4 Pre-strain water level response

The pre-strain water level model is based on the description of a periodic load on a half-space, as described by H. F. Wang (2000), and is used for Earth tides where a vertical head gradient exist (Xue et al., 2016; Allègre et al., 2016). The Equations 14 and 15 were derived from the force equilibrium equations (refer to H. F. Wang (2000))

$$A^e_{M_2} = \frac{1}{S_s}\sqrt{1 - 2\exp\left(-\frac{z}{\delta}\right)\cos\left(\frac{z}{\delta}\right) + \exp\left(-2\frac{z}{\delta}\right)}, \tag{14}$$

and

$$\Delta\phi_{M_2} = \tan^{-1}\left[\frac{\exp\left(-\frac{z}{\delta}\right)\sin\left(\frac{z}{\delta}\right)}{1-\exp\left(-\frac{z}{\delta}\right)\cos\left(\frac{z}{\delta}\right)}\right], \tag{15}$$

where z is depth of the open screen interval, ω is the angular frequency of the tidal component (M_2),

$$\delta = \sqrt{\frac{2D_h}{\omega}}, \tag{16}$$

and D_h is then the hydraulic diffusivity, defined as

$$D_h = \frac{T}{S} = \frac{\langle K\rangle}{S_s} = \frac{k}{\mu S} = \frac{\rho_w g\langle K\rangle}{\mu S_s^p} \tag{17}$$

where T is subsurface transmissivity, k is permeability, $\langle K\rangle$ is hydraulic conductivity, ρ_w is the density of water ($0.9982\ kg/L$ at $20°C$) and μ is the dynamic viscosity of water, S is storativity and S_s^p is specific storage ($1/Pa$). These equations require iterative solving for D_h and S_s.

Equations 14 and 15 were developed for harmonic loading (i.e. ocean or barometric loading) where strain is produced at the surface of the Earth's crust and propagated down (K. Wang & Davis, 1996). ET (tidal dilatation) on the other hand, manifests within the subsurface where the stress is depth independent. Close attention is therefore required for the effect of depth when analyzing combined ET and AT forcing effects (rather than just a loading), ensuring that the sensitivity to depth has adequately attenuated (e.g. deeper than $10m$), as shown in Figure 2.

2.2.5 Distinguishing between pre- and post-strain conditions

The sets of Equations 6 and 7 from Hsieh et al. (1987) describe horizontal flow between the subsurface and the well, whereas Equations 14 and 15 from H. F. Wang (2000) explain the positive phase shift by allowing vertical flow. Both have been used to estimate hydraulic conductivity and specific storage. This is achieved by decomposing the hydraulic diffusivity using the assumptions outlined at the end of Section 2.2.2.

The phase shift determines which of these sets of analytical solutions are appropriate. For a phase between $0°$ to $-45°$ the post-strain response model is used, and for a phase between $0°$ and $90°$ the pre-strain response model is applied (both are visualized in Figure 3). Note that the pre-strain model results in a slight negative phase shift for certain parameter ranges. Consequently, there is a range of ambiguity between phase shift values between $-1°$ to $0°$ in which both sets of solutions should be used, and the

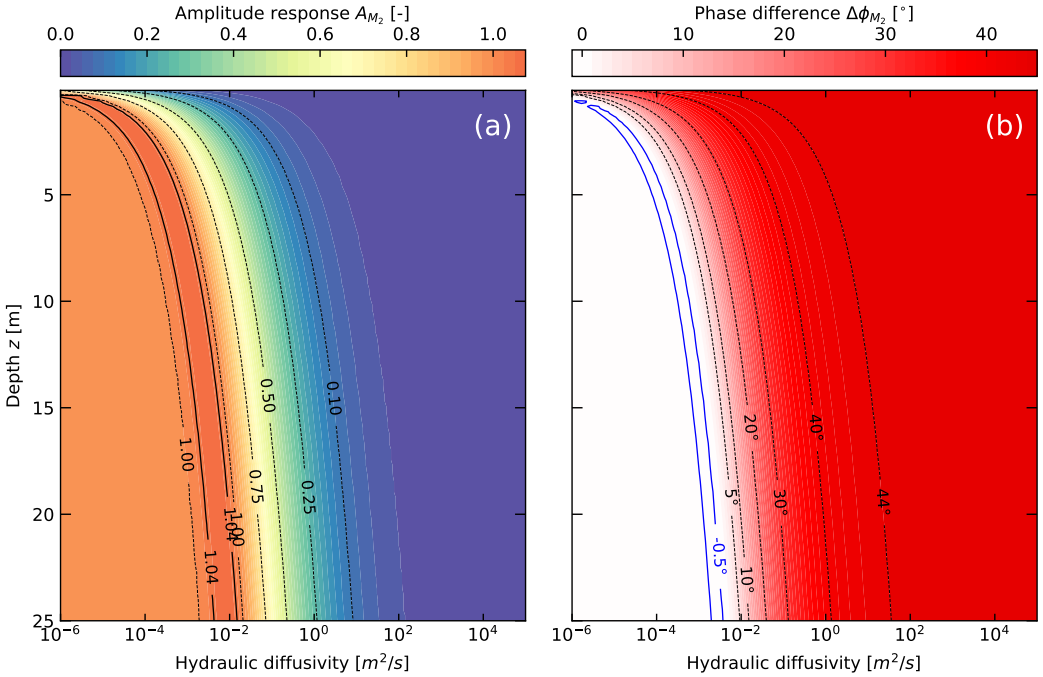

Figure 2. Periodic loading of a half space (applied to ET) as modeled by Equations 14 and 15. (a) Normalized relative amplitude response and hydraulic diffusivity as a function of depth (Equation 14). (b) Phase response and hydraulic diffusivity as a function of depth (Equation 15) H. F. Wang (2000).

most sensible results should be selected (Xue et al., 2016). Note, the unit input as either pressure or hydraulic head will also be carried through the equations resulting in a unit difference where S_s^p is specific storage as pressure $(1/Pa)$ whereas S_s is specific storage as a reciprocal meter length $(1/m)$, as demonstrated in equation 17.

2.3 Atmospheric tide influences on well water levels

Methods that quantify the barometric efficiency of subsurface systems are based on quantifying the groundwater response magnitude to atmospheric pressure changes (Clark, 1967; Rasmussen & Crawford, 1997; Barr et al., 2000; Gonthier, 2003) or atmospheric tides (Acworth et al., 2016). Turnadge et al. (2019) reviewed these methods and concluded that the method by Acworth et al. (2016) was the most robust and reliable. However, their approach was limited by the assumption of an instantaneous and undamped response. Rau et al. (2020) developed a new method that completely disentangles the influences of Earth and atmospheric tides at the same frequency, e.g. S_2. This further

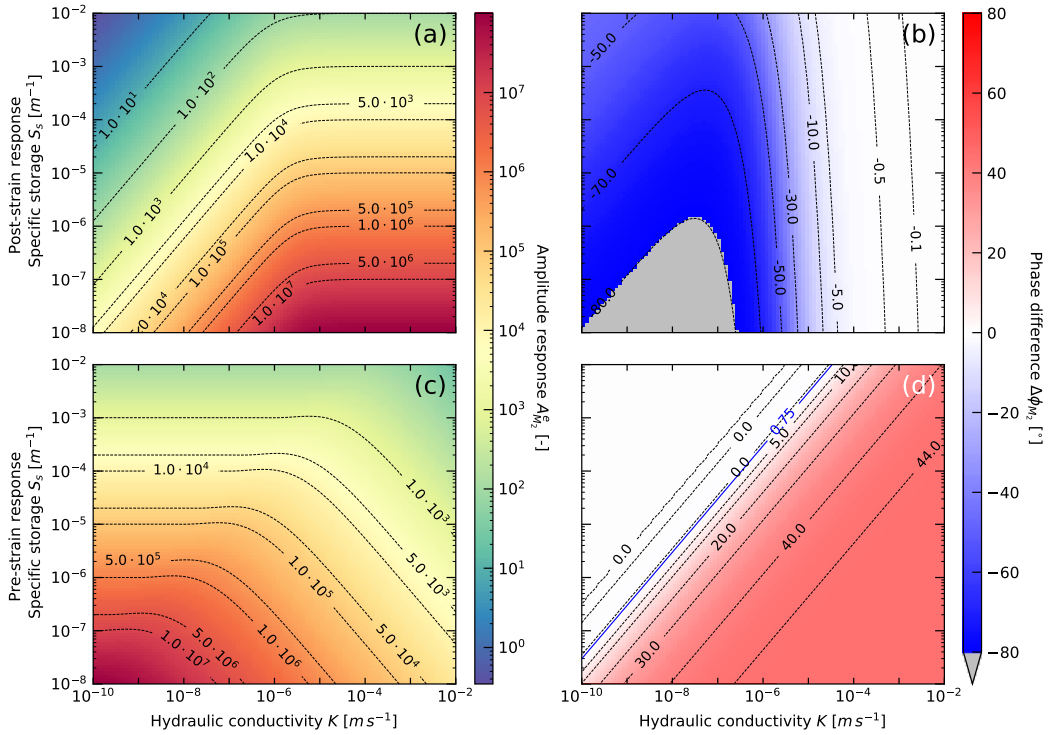

Figure 3. Pressure head amplitude and phase response to the Earth tide M_2 component as a function of ranges in hydraulic conductivity and specific storage: (a) amplitude (Equation 6) and (b) phase (Equation 7) response for confined conditions (here; the radius of borehole and screen are 0.1 m and the screen length is 2 m). (c) amplitude (Equation 14) and (d) phase (Equation 15) response for semi-confined conditions where vertical flow may exist (depth of screen is 20 m).

considers the damping of the subsurface-well system that can be caused by low hydraulic conductivity materials. Their new approach is (Rau et al., 2020)

$$BE_{S_2} = \frac{1}{A_{M_2}} \cdot \left| \frac{\hat{z}_{S_2}^{GW.AT}}{\hat{z}_{S_2}^{AT}} \right|, \tag{18}$$

where

$$\hat{z}_{S_2}^{GW.AT} = \hat{z}_{S_2}^{GW} - \hat{z}_{S_2}^{GW.ET} = \hat{z}_{S_2}^{GW} - \frac{\hat{z}_{M_2}^{GW}}{\hat{z}_{M_2}^{ET}} \hat{z}_{S_2}^{ET}. \tag{19}$$

Here, A_{M_2} corrects for the damping of the subsurface-well system, e.g. for low hydraulic conductivity, and can be inferred from Earth tides as calculated earlier (Equation 4); $\hat{z}_{S_2}^{GW.AT}$ is the S_2 component of the groundwater response to atmospheric tides, and $\hat{z}_{S_2}^{AT}$ is the S_2 frequency component (atmospheric tide) embedded in atmospheric pressure measurements. BE forms a stress balance, described as (Jacob, 1940)

$$BE + \gamma = 1, \tag{20}$$

where γ is the loading efficiency.

2.4 Combining Earth and atmospheric tide responses

2.4.1 General relationships

Within the following derivations it is assumed that Earth tides only induce horizontal areal strain ($\epsilon_a = \epsilon_{11}+\epsilon_{22}$) whereas atmospheric tides only induce vertical strain ($\epsilon_{33} = -p_{AT}$) (Rojstaczer & Agnew, 1989; Cutillo & Bredehoeft, 2011), all of which are assumed to act instantaneously on the subsurface as is consistent with previous literature (H. F. Wang, 2000; Rau et al., 2018). Under such conditions, van der Kamp and Gale (1983) has shown that the rigidity modulus (also known as the shear modulus, G) can be estimated, with the previous outlined assumptions, from combined Earth and atmospheric influences as

$$G = A^e_{M_2}\frac{\rho g}{2\gamma} = A^e_{M_2}\frac{\rho g}{2(1-BE)}, \tag{21}$$

where, $A^e_{M_2}$ originates from Earth tides (Equation 3), whereas BE or γ is derived from atmospheric tides (Equation 20).

The disentanglement of Earth and atmospheric tides from the groundwater well level response, and the use of these separate frequency components to quantify hydro-geomechanical properties allows further geomechanical derivations to be made. Two methods are presented below which solve for the assumption of either incompressible (unconsolidated material) or compressible grains (consolidated material). The choice between which method to use is established by examining an estimated *Biot-Willis* coefficient defined as (H. F. Wang, 2000)

$$\alpha = 1 - \frac{K}{K_s} = \frac{\beta_s}{\beta}. \tag{22}$$

Where K is the Bulk modulus, K_s is the Bulk modulus of the solid grain, β is the compressibility, and β_s the compressibility of the solid grain. For unconsolidated conditions, where the Bulk modulus is much smaller than the Bulk modulus of the grains ($K \ll K_s$) it is possible to assume incompressible grains. The *Biot-Willis* coefficient $\alpha \to 1$ shows that the contribution of the grains to the compressibility of the bulk material is insignificant Rau et al. (2018). By contrast, in consolidated cases K becomes larger, leading to a coefficient that deviates appreciably from one ($\alpha < 1$). In such cases, the grain compressibility is a significant proportion of the total material compressibility and must be accounted for.

316 ### *2.4.2 Incompressible grains*

317 For incompressible grains ($\alpha = 1$) the uniaxial loading efficiency is related to the
318 uniaxial bulk properties as (van der Kamp & Gale, 1983)

$$\gamma = \frac{\beta_v^u}{\theta\beta_f + \beta_v^u}, \tag{23}$$

319 where β_f is the compressibility of the fluid ($4.59\times10^{-10}\ Pa^{-1}$ at $20°C$), β_v^u is the ver-
320 tical undrained bulk compressibility and θ is the total porosity of the formation. The
321 uniaxial specific storage (assuming incompressible) grains is defined by Jacob (1940) as

$$S_s = \rho g(\beta_v^u + \theta\beta_f). \tag{24}$$

322 This equation was used by Acworth et al. (2016), with an S_s estimate from Equa-
323 tion 25, to constrain Equation 24 allowing β_v to be resolved.

$$S_s = \rho_w g\beta_f \frac{\theta}{BE} = 4.5 \times 10^{-6}\frac{\theta}{BE}. \tag{25}$$

324 However, this requires a prior estimate of the porosity θ which is often difficult to de-
325 termine due to the lack of available field measurements. Note also that the above equa-
326 tions assume that barometric loading is uniaxial, and as such use vertical compressibil-
327 ity (β_v) rather than that of the volumetric (bulk) compressibility (β). Here, were instead
328 propose using the S_s derived from the pre- or post-strain response to ET (Section 2.2)
329 to instead constrain Equation 25 to estimate the subsurface porosity by rearranging Equa-
330 tion 25 (similar to Jacob (1940)) as

$$\theta = \frac{S_s BE}{\rho g\beta_f} = \frac{S_s}{\rho g\beta_f}(1-\gamma). \tag{26}$$

331 To achieve a similar outcome as Acworth et al. (2016) this porosity, in addition to the
332 calculated S_s, can now be used in Equation 27, rearranged from Acworth et al. (2016),
333 to provide a uniaxial (vertical) bulk compressibility (inverse vertical undrained bulk mod-
334 ulus (K_v^u)) of the subsurface defined as (Acworth et al., 2016)

$$\beta_v^u = \frac{\gamma\theta\beta_f}{1-\theta} = \frac{1}{K_v^u}. \tag{27}$$

335 This approach is similar to the one used by Cutillo and Bredehoeft (2011) but uses
336 the objective BE method developed by Rau et al. (2020) instead of the subjective cor-
337 relation by Gonthier (2003). Within this subsection it has been shown that it is possi-
338 ble to derive an estimate of porosity from a loading strain if the specific storage is known.

This assumes incompressible grains and is therefore suitable for unconsolidated material (Rau et al., 2019).

The assumption of incompressible grains allows for the removal of the grain compressibility and provide a simplification of the poroelastic space. This step, combined with the new derivation of the shear modulus enables a linear analytical solution of the remaining elastic variables in unconsolidated material ($\alpha \approx 1$). The first step can be taken by deriving the undrained bulk modulus (K_u) with the K_v^u from Acworth et al. (2016) as (H. F. Wang, 2000)

$$K^u = K_v^u - \frac{4}{3}G, \tag{28}$$

which allows for the solving of Skempton coefficient defined as (Rau et al., 2018)

$$B = \gamma \frac{K_v^u}{K^u} = \gamma \frac{\beta^u}{\beta_v^u}. \tag{29}$$

Determination of the Skempton coefficient along with the loading efficiency unlocks the undrained Poisson's ratio using (H. F. Wang, 2000)

$$\nu^u = \frac{3\gamma - B}{3\gamma + B} \tag{30}$$

and drained Poisson's ratio as (H. F. Wang, 2000)

$$\nu = \frac{3\nu^u - B(1+\nu^u)}{3 - 2B(1+\nu^u)}. \tag{31}$$

Knowledge of the drained Poisson ratio further unlocks all remaining poroealastic properties such as Young's Modulus (E), defined as (H. F. Wang, 2000)

$$E = \frac{9KG}{3K + G}. \tag{32}$$

Equations 23-32 define the complete parameter space for unconsolidated materials.

2.4.3 Compressible grains

To solve the poroelastic properties of consolidated materials, the grain compressibility must be considered ($\alpha < 1$). Further, the following two assumptions apply: (1) Although pore fluids technically respond to cubic strains, the areal strain can be used to estimate the subsurface strain from ET; (2) The system is homogeneous and laterally extensive, thus ignoring topographic effects and considering the barometric loading to be uniform. The equations that define the remaining elastic properties for such conditions are (Beavan et al., 1991)

$$B = \frac{3\gamma(1-\nu)}{2\gamma\alpha(1-2\nu) + (1+\nu)}, \tag{33}$$

and

$$\theta = \left(\frac{1}{B} - 1\right)\left(\frac{1}{K} - \frac{1}{K_s}\right)\left(\frac{1}{K_f} - \frac{1}{K_s}\right)^{-1}, \tag{34}$$

and

$$\alpha = 1 - \frac{K}{K_s} = 1 - \frac{2G(1+\nu)}{3K_s(1-2\nu)} \tag{35}$$

and

$$S_s = \frac{\rho g}{\gamma(1-\nu)}\left(\frac{1-2\nu}{2G} - \frac{1+\nu}{3K_s}\right). \tag{36}$$

Equations 33-36 form a non-linear system which must be solved by iteration.

If the petrology of the lithology is known, appropriate literature compressibility values of the dominant grain mineralogy (K_s) could be used. Quartz is the most common naturally occurring mineral and is also one of the least compressible (it is also applicable for most of our case sites), and it will therefore be used to define the upper bounds of K_s here. Richardson et al. (2002) summarized literature values of poly-crystalline quartz for K_s to range between 36-40 GPa, and reported K_s values for the quartz Ottawa Sandstone to be in a range of 30-50 GPa. The average of these ranges has been determined as 42 GPa (Rau et al., 2018) and will be used in this work.

With the established inputs of $\gamma, (BE)$, A_{M_2}, G (Equation 21), S_s and an estimate of K_s, it is possible to simultaneously solve Equations 33-36 for Skempton's coefficient (B), porosity (θ), *Biot-Willis* coefficient (α) and specific storage (S_s) (Beavan et al., 1991). This allows a complete calculation of all remaining poroelastic properties whose interdependency is summarized in Table 2.

3 Method application under different hydrogeological settings

3.1 Field sites, geological context and monitoring

To demonstrate the new method, groundwater and barometric pressure records from four sites and five monitoring bores were used. These sites were selected based on three main criteria: Data availability; a strong M_2 tidal component; and providing different hydrogeological settings with existing studies for parameter comparisons. The Cattle Lane site has unconsolidated materials and was processed using the approach for unconsolidated systems with incompressible grains. All other sites were evaluated by assuming compressible grains. Specific bore geometries and measurements used in the analysis of these sites such as depths and bore construction are summarized in Table 3.

	K Bulk Modulus	K_v Uniaxial Drained Bulk Modulus	ν Poisson's Ratio	E Young's Modulus	G Shear Modulus
K, G	-	$K + \frac{4G}{3}$	$\frac{3K-2G}{2(3K+G)}$	$\frac{9KG}{3K+G}$	-
G, E	$\frac{EG}{3(3G-E)}$	$G\frac{4G-E}{3G-E}$	$\frac{E}{2G} - 1$	-	-
E, K	-	$3K\frac{3K+E}{9K-E}$	$\frac{3K-E}{6K}$	-	$\frac{3KE}{9K-E}$
G, ν	$G\frac{2(1+\nu)}{3(1-2\nu)}$	$G\frac{2-2\nu}{1-2\nu}$	-	$2G(1+\nu)$	-
K, ν	-	$3K\frac{1-\nu}{1+\nu}$	-	$3K(1-2\nu)$	$3K\frac{1-2\nu}{2+2\nu}$
E, ν	$\frac{E}{3(1-2\nu)}$	$\frac{E(1-\nu)}{(1+\nu)(1-2\nu)}$	-	-	$\frac{E}{2+2\nu}$

Table 2. Elastic constant relationships for isotropic stress and undrained conditions (Birch, 1996; H. F. Wang, 2000; Sheriff, 2002). Note that Young's modulus may also be used to provide the uniaxial compression strength (UCS) using the linear relationship work established by Colwell and Frith (2006).

3.1.1 Cattle Lane (NSW, Australia)

Cattle Lane is located on the Liverpool Plains, NSW, eastern Australia. Erosion of the basaltic Liverpool Ranges to the south produced a succession of unconsolidated silts, clays, sands, gravel and minor carbonate nodules within the Liverpool Plains. A thick sequence of clay bound sediments overlie a gravel aquifer at 40 m. This aquifer has previously be shown to respond to loading by rainfall events (Timms & Acworth, 2005). The lithology of the 1 m screened interval was described by Acworth et al. (2015) as major basalt fragments mixed with coarse sand, shell and carbonate nodules. The site has previously been cored to 31.5 m depth, lithologically logged and geophysical surveyed, confirming that it is horizontally extensive (Acworth et al., 2015). Cross-hole seismics were also conducted by Rau et al. (2018) to the depth of 40 m (screened interval of bore BH30061 is 55 m depth, see Table 3), providing depth profiles of elastic variables that were used to constrain the pore pressure response to atmospheric tides analysis.

Further studies at this site include Acworth et al. (2016) and Acworth et al. (2017), which were precursors to Rau et al. (2018) in the investigation of pore pressure response

Borehole	**Inputs**								**Description**	
	A_{M_2}	A^e	ϕ_{M_2}	r_c	r_w	b	z	K_s	Lithology	Strain
Cattle Lane; BH30061	0.765	$4.56 \cdot 10^4$	24.9	*0.125*	*0.12*	*1*	55	-	Sand, Gravel, Clay	Pre
Dodowa; BH11	0.907	$1.30 \cdot 10^6$	-13.8	0.058	0.048	2	*45*	42	Gneiss	Post
Thirlmere; GW075409.1.2	0.999	$3.24 \cdot 10^5$	10	*0.156*	*0.14*	*12*	78	42	Quartz arenite sandstone	Pre
Thirlmere; Thirlmere 2	0.986	$3.52 \cdot 10^5$	-4.7	0.114	0.108	4	*72*	42	Quartz aranite sandstone	Post
Death Valley; BLM-1	0.998	$1.48 \cdot 10^6$	-1.1	0.127	0.127	106	*830*	42	Carbonate	Post

Table 3. Inputs parameters for case sites where; A_{M_2} is the dimensionless amplitude response, A^e is the amplitude response, ϕ_{M_2} is the phase shift of the M_2 component, r_c is the outer diameter (m) of the bore casing, r_w the internal diameter (m) of the bore casing, b is the Aquifer thickness (m) or open interval of the screen, z is the depth (m) to the center of the screen or open interval, and K_s is the assumed grain bulk modulus. Italicized values were not used in the applied pre- or post-strain models, but are provided for context.

to atmospheric tides, and Timms et al. (2018) on a core scale analysis of the site's laterally extensive and thick aquitard. In this paper, time-series data of groundwater pressure heads were used from the bore BH30061 due to the strong M_2 signal, between the 21/01/2016 and 14/04/2018, located at latitude $-31.518340°$, longitude $150.468332°$ and an height of 313 MASL (WGS84). The groundwater pressure heads were collected using vented In-Situ Troll 700H series loggers at hourly intervals. Atmospheric pressure was measured by an In-Situ Baro Troll absolute gauge transducer.

3.1.2 Thirlmere Lake (NSW, Australia)

Thirlmere Lakes is located in the south-west of the Sydney Basin, NSW. Both bores are located in the quartz arenite Hawkesbury sandstone, which is about 100 m thick at the site. This sandstone is deposited by a braided river with the heterogeneous deposits showing overlapping and self incised fining up sequences, with over-bank deposited fines at paleo-channel boundaries (Miall & Jones, 2003). There is evidence that the upper portion of bore Thirlmere 2 passed through a geological fault damage zone, with drilling fluid losses recorded above the screened interval due to fractures (Impax, 2019). Other studies in the same lithology include Ross (2014), which investigated the potential for a bore field development within the Hawkesbury Sandstone, however, no publicly available studies exist for this lithology at the case site.

The time span and collection of the time-series data for the two bores differ. The time-series for GW075409.1.2 was downloaded for the time period of 03/07/2018 to 14/12/2018 from the *WaterNSW* real-time data portal with 15 min intervals, and is located at latitude -34.230666^o, longitude 150.543996^o, height 314 MASL (Russell, 2012). The time-series data for Thirlmere 2 was collected by a university deployed vented In-Situ Troll 700H series pressure transducer every 5 min between the 32/07/2019 and 29/10/2019, and is located at latitude -34.220836^o, longitude 150.536467^o, height 323 MASL. The university deployed loggers were accompanied with downhole barometric loggers, whereas for the WaterNSW bore a matching barometric time-series was obtained from a weather station approx. 500 m away.

3.1.3 Dodowa (Ghana)

Dodowa is located in the Shai Osudoku District in the southeastern part of the Greater Accra Region, Ghana. The local geology consists of the Togo Structural and Dahomeyan Structural units. The Togo being composed of a series of metamorphic and folded quartzites, phyllites and schists, and the Dahomeyan of altered belts of acid and basic gneisses. BH11 used within this paper is located in a Dahomeyan gneiss (Attoh et al., 1997). All units within the region appear highly weathered, resulting in an 5 m unconsolidated regolith with the groundwater table 5 m below the land surface.

BH11 was installed and previously studied by Foppen et al. (2020), including atmospheric tide analysis. The time-series for the water levels of BH11 was collected at 20 min intervals between the 18/10/16 and 07/06/2017 using Mini-Diver DI501; Schlumberger pressure transducers, with atmospheric pressure being recorded with a Mini-Diver DI500; Schlumberger barometric diver, located above ground at the site at an approximate latitude 5.881675, longitude −0.097244, height 88 MASL (Foppen et al., 2020).

3.1.4 Death Valley (California, USA)

The Death Valley site is located in the western part of the USA on the border of Nevada and California at a position of; latitude 36.408130, longitude -116.471360 (WGS84), elevation 688 MASL. Bore BLM-1 is located in Paleozoic carbonate rock and was left as an open well. The same time-series record was also used in Rau et al. (2020) and it is the same wellbore for which data was analysed in Cutillo and Bredehoeft (2011). Data was recorded at 15 min intervals using an In Situ Troll with a vented cable and an In Situ Barotroll. The time-series extends between the 25/06/2009 and 16/12/2009.

3.2 Method application

Groundwater pressure head and barometric pressure time-series were recorded at sub-hourly intervals at all sites (e.g. Figure 4) for at least three months which is longer than the $\sim$ 28 days being suggested as the minimum requirement (E. Roeloffs, 1996). The theoretical Earth tide potential for the same duration and sampling frequency of each site was calculated using *PyGTide* (Rau, 2018). This required knowledge of the geoposition of the borehole (latitude, longitude and height in WGS84). Additional information required for the analysis, such as casing and screen radius's, screen depth and

length, were also noted for each bore and were presented in Table 3. All time-series were detrended by a moving 3 day average using the *SciPy* detrend function, and the tidal main tidal components were extracted using *HALS* (Section 2.1).

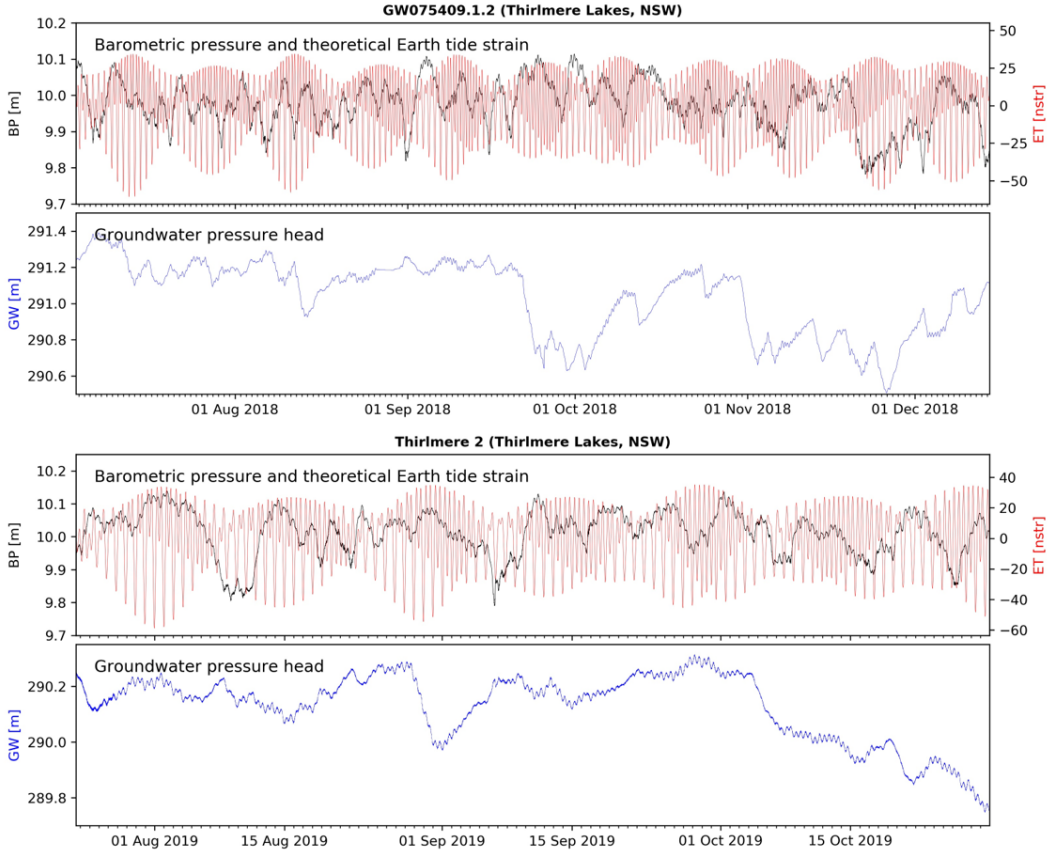

Figure 4. Time-series of barometric pressures (m), theoretical Earth tide nanostrain (nstr) and groundwater levels from bores GW075409.1.2 and Thirlmere 2 from Thirlmere Lakes, NSW, Australia.

The following offers a step-by-step summary of the method:

1. Calculate the theoretical Earth tide potential time-series for the location and same time duration and interval of collected groundwater and barometric pressure data with reference to Coordinated Universal Time (UTC).
2. Calculate the spectra using the harmonic least squares and extract the dominant tidal components M_2 and S_2 for barometric and groundwater pressure heads as well as Earth tide potential.

3. For the M_2 component, convert the tidal potential to dilatation strain and calculate the amplitude responses.
4. Compute the phase shift between the groundwater and Earth tides. A negative phase shift points to a post-strain groundwater response and the Equations 6 and 7 from Section 2.2.3 should be used. A positive phase shift indicate a pre-strain response and Equations 14 and 15 from Section 2.2.4 should be used. Evaluate hydraulic conductivity ($\langle K \rangle$) and specific storage (S_s) using either the post or pre-strain models described in Sections 2.2.3 or 2.2.4 depending on negative or positive M_2 phase shift between ET and GW respectively, as shown in Figure 5.
5. Calculate the barometric efficiency (Equation 18) using the normalized Amplitude response (Equation 4, and the shear modulus (Equation 21) using the amplitude response to tidal dilation strain (Equation 3).
6. Distinguish between unconsolidated and consolidated systems:

   a Unconsolidated: This assumes incompressible grains ($K_s \to \infty$ and $\alpha = 1$). BE is then combined with the specific storage output from either Section 2.2.3 or 2.2.4 (depending on whether the phase is positive or negative) to solve for porosity using Equation 26 assuming incompressible grains.

   b Consolidated: This assumes compressible grains ($K_s < \infty$ and $\alpha < 1$). For consolidated conditions, the BE is converted to a loading efficiency by using Equation 20, a shear modulus derived using Equation 21, and combined with the specific storage, dilatation strain, and an assumed solid grain compressibility to simultaneously solve Equations 33 to 36.

7. All remaining poroelastic properties whose relationships are shown in Table 2 may then be derived, e.g. Young's modulus (E) using Equation 32.

In this paper, all of the methodology and equations were implemented in the *Python* programming environment, and joint iterative solving was completed with *SciPy*'s *curve_fit* function which applies least-squares while considering realistic parameter bounds ($0 \leq B \leq 1$, $-1 \leq \nu \leq 0.5$, $0.005 \leq G \leq 40$ GPa, $0 \leq \theta \leq 0.5$). We note that fitting did not exceed any of the prescribed bounds for any of the analysed data sets.

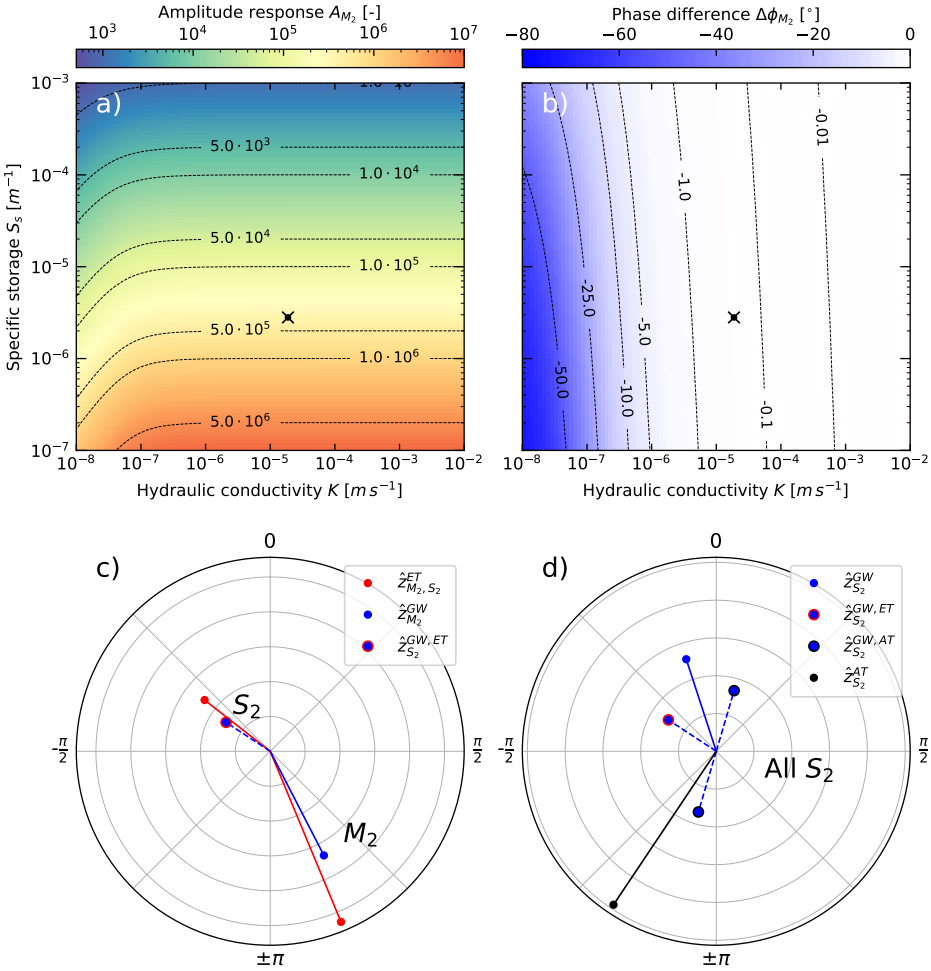

Figure 5. Phase and amplitude responses from the processing of bore Thirlmere 2; a) and b) plot (black dot) the amplitude ratio and phase shift relationships between the subsurface pore pressure and well water level for the post-strain Earth tide model (Section 2.2.3), c) and d) are polar plots showing the amplitude and phases of the complex inference of the well response to Earth tides from the response at M_2, and the disentanglement of the well response at atmospheric tide S_2, respectively.

3.3 Hydro-geomechanical properties

The hydro-geomechanical properties for the field sites from the application of the method outlined in Section 3.2 are presented in Table 4. The boreholes BH30061 and GW075409.1.2 from Cattle Lane and Thirlmere Lakes produced positive M_2 phase shifts (Table 3), with specific storage and hydraulic conductivity therefore being derived from the Pre-strain model (Section 2.2.4). All other bores had negative phase shifts and were

processed using the Post-strain model (Section 2.2.3) from Hsieh et al. (1987). BH30061 was the only data set processed using the proposed unconsolidated analytical model. If applying the assumed grain compressibility of quartz ($K = 42$ GPa) for BH30061, a *Biot-Willis* coefficient of 0.99 is obtained and hence justifies the assumption of incompressible grains ($\alpha \approx 1$) (Section 2.4.2). Both the quartz sandstone bores returned *Biot-Willis* coefficients of 0.96, and the gneiss bore 0.84, as such, these bores required a value for the grain compressibility (Section 2.4.3).

3.3.1 Cattle Lane (NSW, Australia)

The specific storage, hydraulic conductivity, porosity, shear modulus, and undrained Poisson's ratio from Cattle Lane are consistent with literature values for the sediment type (Bowles, 1996), and comply with previous estimates from higher in the stratigraphy at the same site obtained by cross-hole seismics (Acworth et al., 2015, 2016; Rau et al., 2018). The Young's modulus of 0.34 GPa deviates from the expected material range reported in the literature for an unconsolidated clay, sand and gravel mixture of between 0.025 and 0.2 GPa, although is reasonable when considering consolidation at 55 m depth and an in-situ derivation (Bouzalakos et al., 2016). The Poisson's Ratio of -0.31 is the only parameter that deviates significantly from the expected range of 0.2 to 0.5. This will be discussed later.

3.3.2 Thirlmere Lakes (NSW, Australia)

Estimates of hydrogeomechanical parameters (S_s of $1.5{\cdot}10^{-6}$ and $9.1{\cdot}10^{-7}$ $(1/m)$; $\langle K \rangle$ of $2.8{\cdot}10^{-7}$ and $1.9{\cdot}10^{-6}$ (m/s)) for the two quartz sandstone bores are considered realistic for a quartz sandstone in this area. The higher $\langle K \rangle$ for Thirlmere 2 is believed to be indicative of enhanced hydraulic conductivity due to fractures. For this sandstone formation, SCA (2005, 2006) has previously reported S_s values of $2.49 \cdot 10^{-6}$ to $2.41 \cdot 10^{-4}$ $(1/m)$ and $\langle K \rangle$ of $1.15 \cdot 10^{-6}$ to $3.36 \cdot 10^{-6}$ (m/s) within this formation, including fracture networks (Ross, 2014). Geomechanical estimates of the shear modulus of 2.64 GPa marginally exceeds the expected range of $1-2$ GPa (Bertuzzi, 2014; C. Zhang et al., 2016; C. Zhang & Lu, 2018). Conversely, the bulk modulus and Young's modulus both fall within the expected ranges of 2.6 to 5.3 and 3 to 8 GPa, respectively. The

Location / Borehole	**Results**										
	$< K >$	S_s	BE	θ	G	ν	ν_u	K	B	E	α
Cattle Lane / BH30061	$5.4 \cdot 10^{-6}$	$1.7 \cdot 10^{-5}$	0.08	0.39	0.25	-0.31	0.46	0.07	0.98	0.34	0.99
Dodowa / BH11	$2.6 \cdot 10^{-6}$	$7.3 \cdot 10^{-7}$	0.74	0.09	24.10	-0.23	0.06	8.47	0.70	37.10	0.80
Thirlmere / GW075409.1.2	$2.6 \cdot 10^{-8}$	$3.1 \cdot 10^{-6}$	0.40	0.25	2.62	-0.04	0.36	1.56	0.85	5.04	0.96
Thirlmere / Thirlmere 2	$1.9 \cdot 10^{-5}$	$2.8 \cdot 10^{-6}$	0.35	0.19	2.64	-0.03	0.38	1.62	0.88	5.13	0.96
Death Valley / BLM-1	$4.2 \cdot 10^{-6}$	$6.7 \cdot 10^{-7}$	0.60	0.06	24.10	-0.22	0.18	8.47	0.70	28.28	0.84

Table 4. Results from case sites where; $\langle K \rangle$ is hydraulic conductivity (m/s), S_s is the specific storage $(1/m)$, BE is the barometric efficiency, θ is porosity, G is the shear modulus (GPa), ν is Poisson's Ratio, ν_u is the undrained Poisson's Ratio, K is Bulk Modulus (GPa), B is Skempton's coefficient, E is Young's modulus (GPa) and α is the *biot-willis coefficient.*

estimated Poisson's ratios of -0.04 and -0.03 are low compared to values between 0.2 and 0.3 typically measured in the laboratory (McMillan et al., 2019).

3.3.3 Dodowa (Ghana)

The hydrogeomechanical estimates of hydraulic conductivity of $2.6 \cdot 10^{-6}$ (m/s) and specific storage of $7.3 \cdot 10^{-7}$ $(1/m)$ are comparable with the values for the Togo Structural Unit from Foppen et al. (2020) derived from pumping and slug tests, which indicated ranges between 10^{-5} to 10^{-6} (m/s), and $2.3 \cdot 10^{-7}$ to $7.7 \cdot 10^{-8}$ $(1/m)$, respectively. The estimated porosity of 0.09 for BH11 slightly exceeds the range of 0.005 to 0.05 in Foppen et al. (2020). Comparison of elastic modulus is problematic for schists, as values are dependent on the original protolith and may vary significantly, and because schistose rock masses are known for high values of anisotropy (Hoek & Diederichs, 2006). For example, Young's modulus for a schist, as in the screened interval of BH11, can vary significantly between 21 to 117 GPa depending on mineralogy and foliation orientation (Condon et al., 2020). Our estimated value of 37.1 GPa falls within this range. However, detailed mineralogy does not exist for this bore to allow a closer comparison with literature values.

3.3.4 Death Valley (California, USA)

The estimated hydraulic conductivity of $4.2 \cdot 10^{-6}$ (m/s), is in agreement with the Earth tide analysis derived value of $1.3 \cdot 10^{-6}$ (m/s) by Cutillo and Bredehoeft (2011). In contrast, the estimated specific storage value of $6.7 \cdot 10^{-7}$ $(1/m)$ is in disagreement with the value of $7.3 \cdot 10^{-6}$ $(1/m)$ by Cutillo and Bredehoeft (2011). However, the specific storage and hydraulic conductivity values are both consistent with the values published by Rau et al. (2020) for the same dataset, using the same ET method. The porosity determined by this paper (0.06) also aligns with the lower end of the range proposed by Cutillo and Bredehoeft (2011), it is reasonable to assume the calculated Young's and shear modulus of 28.28 and 24.10 GPa are similarly plausible (Parent et al., 2015). We note that the derived Poisson's ratio of -0.22 differs significantly from the value of 0.25 which was merely assumed in Cutillo and Bredehoeft (2011).

4 Discussion

4.1 Harmonic disentanglement allows estimation of the poroelastic parameter space

In this work, we make use of recent advances that allow quantitative disentanglement of the groundwater response to both Earth and atmospheric tidal forces. Since each mechanism acts differently on the subsurface, the disentangled responses can be merged through theoretical relationships. Unlike previous research, this allows the solving of the complete poroelastic space for unconsolidated systems entirely based on time-series of measured groundwater pressure heads, atmospheric pressure, and calculated Earth tides. For consolidated systems, the complete poroelastic space can also be solved through a system of nonlinear equations by assuming the grain compressibility. This approach has previously been used in Rau et al. (2018).

A general agreement is held throughout the literature that a negative phase shift is representative of an observed time lag caused by the slow flow of fluid from the formation into the bore, in response to the tidal strain (Bower, 1983; Hsieh et al., 1987; Kümpel, 1997; Schulze et al., 2000). Conversely, no such agreement is held for positive phase shifts. Although Section 2.2.4 is based on the assumption that positive phase shifts relate to vertical flow to the water table, i.e. semi-confined conditions (E. A. Roeloffs et al., 1989), other explanations for positive phase shifts exist within the literature. These include the influence of fracture transmissivity and length, ocean loading, heterogeneous material properties and topographic effects (E. Roeloffs, 1996; Burbey, 2010). Here, positive phases from either vertical flow or fracture flow describe a process in which pressure is able to be propagated rapidly, either to the water table or along a highly transmissive fracture (Bower, 1983). Other mechanisms for phase shifts have also been explored in the broader literature, such as Hanson and Owen (1982), who related fracture orientation (strike and dip) to either positive or negative phase shifts.

In this study, positive and negative phases shifts were recorded at the various field sites. A comprehensive understanding of negative and particularly positive phase shifts is still lacking within the literature. Shi and Wang (2016) observed that negative phase shifts were indicative of predominantly horizontal groundwater flow in a completely undrained system, while a positive phase shift was indicative of a vertical hydraulic gradient in a semi-confined or unconfined system. The method by Hsieh et al. (1987) outlined above

as the post-stain model (negative phase shift), which was used by Shi and Wang (2016), is based on the assumption of radial horizontal flow into a well. If a positive rather than negative phase shift is used as an input into the system of equations provided by Hsieh et al. (1987), the results will not be sensible. As such, a positive phase shift model is required. For this project the method provided by H. F. Wang (2000), and adapted by Xue et al. (2016) and Allègre et al. (2016), was implemented to account for vertical flow. This method, as described in Section 2.2.4, was developed for a subsurface forcing by harmonic surface loading. Earth tides do not act by surface loading but rather the mechanism is tidal dilatation, where gravitational forces act on mass across the vertical profile. Although the method based on positive phase shifts has been successfully applied within the literature, the validity of this model has not yet been proven and further research is necessary.

Previous methods that utilized EAT for subsurface characterization have always required the assumption of an elastic modulus, typically Poisson's ratio, to resolve additional geomechanical parameters of the subsurface. The outlined method in this study has removed this assumption by allowing the Poisson's Ratio to be calculated as part of the TSA. Primarily it is the prior estimate of the specific storage (also determined by TSA) which allows the Poisson's Ratio, along with all the other parameters, to vary within the theoretical ranges. As such, a relationship can be established between phase and amplitude in the methodologies presented here. Within the post-strain model (Section 2.2.3, Hsieh et al. (1988)) a decrease in phase (larger negative number) acts to decrease both the hydraulic conductivity and specific storage, whereas for an increase in the amplitude response the hydraulic conductivity remains stable (marginally increases) and the specific storage decreases. This can be summarized as:

$$\phi \downarrow = \langle K \rangle \downarrow,\ S_s \downarrow;\ amp \uparrow = \langle K \rangle \sim,\ S_s \downarrow \tag{37}$$

For the pre-strain model (Section 2.2.4, H. F. Wang (2000)) an increase in phase difference increases the hydraulic conductivity and decreases the specific storage, and an increase in the amplitude response increases the hydraulic conductivity but decreases the specific storage, summarized as:

$$\phi \uparrow = \langle K \rangle \uparrow,\ S_s \downarrow;\ amp \uparrow = \langle K \rangle \uparrow,\ S_s \downarrow \tag{38}$$

Within the compressible grains model (Section 2.4.3), an increase in amplitude response results in an increase in the shear modulus and a decrease in the porosity. Whereas an

increase in barometric efficiency (i.e. smaller loading efficiency) results in an increase of both the shear modulus and porosity, summarized as:

$$amp \uparrow = G \uparrow,\ \theta \downarrow;\ BE \uparrow = G \uparrow,\ \theta \uparrow \tag{39}$$

However, this is compounded with the change in the specific storage from either an increase or decrease in the amplitude response. Note the importance of this relationship and the effect of the S_2 disentanglement by Rau et al. (2020), whereby comparison previous methods which calculated BE such as Jacob (1939) or Acworth et al. (2017) overestimate the barometric loading. This in turn results in an overestimate of the shear modulus, which would also affect the derivations of other parameters according to Equation 21.

4.2 Strain responses reveal subsurface heterogeneity and anisotropy

Combining ET and AT responses in the subsurface analysis is based on the principle that Earth and atmospheric tides induce strains with a different directionality. ET is fundamentally cubic, but is approximated as planar (tidal dilatation) (Schulze et al., 2000; Fuentes-Arreazola et al., 2018). However, Rojstaczer and Agnew (1989) stated that the use of the horizontal areal strain from Earth tides is a sufficient approximation for subsurface depths of up to thousands of kilometers. For ET, the strain is experienced in the vicinity of the well bore screen, although the distribution of this stain radially (cylindrical or spherical) from the screen is uncertain. The subsurface strain response to Earth tide induced stress depends on the elastic properties which are highly heterogeneous on a small scale. However, the pore pressure response as measured by a well intersects a larger volume and should therefore be representative of the theoretical values derived from Earth tide calculations.

Rojstaczer and Agnew (1989) predict that the response of ET (areal strain) should be high for low porosity and compressibility. Similarly, for such conditions, the barometric efficiency should approach one ($BE \rightarrow 1$, or equivalently $\gamma \rightarrow 0$). However, this does not necessarily occur as can be seen in our results for Death Valley and Dodowa where the groundwater response magnitude to ET is large but BE is significantly smaller than unity. This phenomenon can be explained by the fact that BE is estimated vertically across a typical geological profile as a surface load, uniaxially compressing the subsurface. Here, consolidation generally increases with depth and we hypothesize that the

AT response vertically integrates the material properties above the monitoring point, i.e. the result is representative of the vertical heterogeneity in elastic properties encountered. The precise geometry of the representative volume from either ET or AT is currently unknown, but it is assumed to be equivalent. However, if this assumption is flawed and the representative volumes of ET or AT significantly differ, strain anisotropy may exist between these two forces and complicate their joint interpretation. Detailed field experimentation or coupled hydraulic-geomechanical modeling would be required to explore such a phenomenon.

4.3 In-situ conditions explain discrepancy in poroealastic properties

Our results in Table 4 largely comply with previously established values (H. F. Wang, 2000), except for the observation of negative Poisson's ratios. It is important to note that previous studies typically assume a literature value for Poisson's ratio when calculating geomechanical properties (Cutillo & Bredehoeft, 2011). Our new approach is enabled through tidal disentanglement to remove the need for such an assumption. However, the negative Poisson ratios are a surprising result and require explanation.

It is theoretically possible for Poisson's ratio to range between negative one and positive half, i.e. $-1 \leq \nu \leq 0.5$ (R. Lakes, 1991; R. S. Lakes & Witt, 2002). Here, materials with a negative Poisson's ratio are described as auxetic, i.e. materials that become thicker parallel to the direction of the stress. The occurrence of auxetic behavior in rocks was discussed by Gercek (2007), who summarized that as a Poisson's ratio becomes increasingly negative ($\nu \rightarrow -1$), the material become highly resistant to shear deformations but easy to deform volumetrically. Ji et al. (2018) succinctly describe this relationship for conditions where the shear modulus is much greater than the bulk modulus, defined as $K < 2G/3$, and geologically is likely associated with highly anisotropic rocks. This ratio between the bulk and shear modulus is consistent with all results presented in this paper. As such, the negative Poisson's ratios are indicative of the subsurface laterally contracting while being vertically compressed, following the theory of linear poroelasticity.

Previous instances of negative Poisson's ratios for standard uniaxial core sample testing have been recorded by Homand-Etienne and Houpert (1989) and Zhao et al. (2020) in thermally induced micro-cracked granites. However, reporting of auxetic behavior in

rock is dominated by studies involving low strains and low confining pressures. For example, in the Berra Sandstone, Handin et al. (1963) observed that small compressive strains (here, small was defined as less than 200 Bar $\approx$ 2000 mH_2O or 20 MPa) for confining pressure conditions cause the dilation of pore spaces. Comparatively, observations of pore volumes remained constant for moderate strains (20 to 50 MPa) and reduced in volume for large strains ($>$ 50 MPa). Ji et al. (2018) have recently examined auxetic behavior over a broad range of lithologies and pressures. They concluded that negative Poisson's ratios are possible in crystalline igneous and metamorphic rocks (non-fractured) for confining hydrostatic pressures less than 5 MPa, and less than 200–300 MPa for more quartz-rich sedimentary rocks such as silt stones and sand stones. Further, Ji et al. (2018) observed that the porosity of sedimentary rocks plays an important role in controlling auxetic effects, similar to the nano-scale fabric in artificial auxetic materials (e.g. metallic foams).

The results in this paper are obtained in-situ for fully saturated, undrained (confined) conditions and caused by small magnitude strains, which are conditions that differ considerably from those used in traditional laboratory techniques for determining elastic moduli (i.e., E, G, K, ν). Compared to the conditions experienced during a compressive laboratory test, or those described above by (Ji et al., 2018), the strains caused by EAT are very small. For example, the loading variations caused by the atmospheric tidal component S_2 is typically less than $9{\cdot}10^{-5}$ MPa (0.1 mH_2O), and the confining pressure caused by an artesian standing water level of 100 mH_2O equates to a confining pressure of only 0.98 MPa. Laboratory results are also well known for demonstrating bias in the sample strength, with the strength decreasing with the sample's increasing physical size. It has been found that this occurs due to the incorporation of heterogeneities in the sample at larger scales, such as minor lithological changes or discontinuities due to fracturing or jointing (Cundall et al., 2008; Masoumi et al., 2016).

Alternative subjective in-situ methods, such as seismic based methods, still derived positive Poisson's ratios when passing through the same heterogeneous material at the same confining pressures. However, elastic moduli have previously been shown to be frequency dependent when saturated and under confining pressure (H. F. Wang, 1993; Tutuncu et al., 1998). Here, we hypothesize that the low frequency of the EAT induced stresses ($2cpd \approx 2.3{\cdot}10^{-5}Hz$), compared to seismic propagated waves (1 to 100 $Hz \approx$ 86,400 to 8,640,000 cpd), causes a highly relaxed response which allows sufficient time for pres-

sure redistribution (Tutuncu et al., 1998). In contrast, the seismic frequency produces a localized unrelaxed or undrained response as the seismic waves pass through the subsurface, where this effect has been shown to change with the frequency (Pimienta et al., 2016). Both (Tutuncu et al., 1998) and (Pimienta et al., 2016) provide evidence of decreasing Poisson's ratios with decreasing frequency when below the typical undrained response domain ($< 10\ Hz \approx 864,000\ cpd$).

For small strains, as relevant for this study, Zaitsev et al. (2017) have shown that the occurrence of negative Poisson's ratios is not as exotic as previously thought. Considering the context of Cundall et al. (2008), Gercek (2007) and Ji et al. (2018), the negative Poisson's ratios derived by TSA in this paper seem plausible. Here, we propose that these are due to an interplay of simultaneous conditions for the in-situ determination, such as the scale of the effective sample size, anisotropic strain responses from heterogeneities, low confining pressures, and the low frequency and small strains caused by EATs. Meeting the requirements of a negative Poisson's ratio at these small strains defined by (R. Lakes, 1991) as non-affine deformation (non-uniform between scales), non-central forces, and in a state of pre-existing strain (e.g., from overburden). The geomechanical derivations of this paper (Section 2.4) are based on linear poroelasticity. However, the auxetic responses observed by Ji et al. (2018) occurs both linearly and non-linearly within the negative Poisson's ratio space, depending on the confining pressure and the type of material (Zaitsev et al., 2017). Currently, no relationships between EAT and nonlinear poroelastic theory has been established within the literature. Future work in this space should therefore consider the integration of nonlinear geomechanics (Khan et al., 1991; Johnson & Rasolofosaon, 1996).

To the best knowledge of the authors no explicit or robust relationships exist in the literature between elastic moduli results obtained in the field to those estimated from the laboratory testing of core (Leriche, 2017). Similarly, no in-situ method currently exists that can derive elastic estimates of thousands of cubic meters of material (e.g., meters around a well bore screen), as has been proposed for Earth tides (S. Zhang et al., 2019). Over such a large volume, heterogeneity within almost any geological media will produce an anisotropic strain response to either Earth or atmospheric tides. Such anisotropy may result in apparently atypical properties, such as negative Poisson's ratios, and should be investigated for the generic assumption common to most hydro- or geomechanical investigations of a homogeneous, isotropic aquifer of infinite lateral extent.

4.4 Implications for passive quantification of subsurface hydro-geomechanical properties

There are several uncertainties associated with the findings of this paper, with implications for passive quantification of subsurface hydro-geomechanical properties. These uncertainties and limitations of the method are as follows:

- Although subjective estimates have been attempted (S. Zhang et al., 2019), the size and scale of the volume of influence from either ET or AT are unknown. It is also possible that there is a difference between the size of influence for ET and AT. Further research is required to elucidate the zone of influence the derived properties are representative for.
- Currently the poroelastic response to EAT is considered to be linear. However, rocks have previously been shown to respond in a nonlinear manner for undrained, tri-axially loaded laboratory settings, particularly at small strains (Johnson & Rasolofosaon, 1996; Zaitsev et al., 2017). As in-situ derivations of rock mass (or sediment) poroelastic values without the use of assumed primary values (E, G, K, ν) is relatively novel, the implication of assuming linearity for the analysis of in-situ properties remains unknown and unverified.
- The mechanism behind pre-strain responses is believed to be due to a partial drained response in the subsurface. However, the exact causes of such responses are still unknown. In order for the validity of a positive phase shift model to be proven, a more comprehensive understanding of such mechanisms must be further developed.
- Skin and well bore storage effects have been assumed to be negligible in this paper. However, these two effects will alter the phase responses to either Earth or atmospheric tides, as was shown in the recent work by Gao et al. (2020). Although the effect of phase on the geomechanical derivations of this paper is expected to be minor, additional consideration of skin and well bore storage effects will increase the accuracy and confidence in results.

Passively characterizing the subsurface with in-situ measurements may fundamentally change the way in which the confined subsurface is understood. For example, the possibility of auxetic behavior of subsurface materials could change how we estimate compaction associated with groundwater extraction and the behavior of aquifers during man-

aged aquifer recharge. Here, the low strain elastic estimates from TSA may provide a lower bounding end-member for plausible ranges of properties. With further study, it may be possible to infer poroelastic properties at different confining pressures and frequencies or to provide a more accurate in-situ determination of geomechanical rock properties (e.g. specific storage, strength, etc.) prior to excavation and construction of civil and mining projects.

5 Conclusions

The method developed in this paper provides a comprehensive approach to estimate in-situ hydro-geomechanical properties using Tidal Subsurface Analysis (TSA), i.e. from the monitored groundwater response to Earth and atmospheric tides (EAT). Our new method first objectively disentangles the groundwater response to Earth tides (ET) and atmospheric tides (AT) for the dominant response frequencies (M_2 and S_2). Secondly, the approach uses the amplitude and phase responses to ET and AT to determine the complete hydro-geomechanical parameter space: Specific storage, hydraulic conductivity, porosity, shear, Young's and bulk modulus, undrained and drained Poisson's Ratio, Skempton's and Biot-Willis coefficients. Unlike previous research, our new approach does not require an a priori estimate of the Poisson's ratio. However, the application to consolidated systems requires an estimate for the grain compressibility for which literature based values can be used.

Application of our new method to five groundwater and barometric pressure records from four different hydrogeological settings delivers physically realistic results that are consistent with previous estimates. However, we reveal that the in-situ estimates of Poisson's ratio are consistently negative indicating auxetic behavior. A closer look at the literature reveals that this is not unrealistic and can be attributed to an interplay between simultaneous in-situ conditions that differ from those of established laboratory tests. These include a larger effective sample size with scaling effects, anisotropic strain responses due to heterogeneities (e.g., micro-cracking), significantly lower confining pressures, and the small strains at low frequencies caused by the EATs.

Our approach allows estimation of the complete hydro-geomechanical parameter space in a passive way, i.e. from monitoring records of groundwater pressure head, measured atmospheric pressure and calculated ET. The primary advantage is that all pa-

rameters are determined for the same in-situ conditions and that the estimated values therefore should be internally consistent. The new method enables site-specific heterogeneity to be evaluated, as was shown by the two evaluated records from sandstone bores, providing hydro-geomechanical properties of the rock mass rather than small scale estimates on intact rock. This is a clear advantage to methods that require taking samples to the laboratory where replicating field conditions such as in-situ confining pressure and representative scale can be problematic. However, our method also raises the need for further research in key areas where significant uncertainties remain, for example the possibility for non-linearity of the poroelastic response to surface loading and Earth tide forces. Addressing the identified uncertainties could contribute towards improving subsurface monitoring and characterization in both consolidated and unconsolidated systems.

Acknowledgments

GCR and TCM conceived the idea for this paper. TCM and GCR analysed the data and made the figures. MSA and WAT contributed with datasets and suggested improvements. All data used in this paper are available from the authors upon request. Data will be cited and made available in a FAIR aligned repository upon acceptance of this manuscript.

Thanks are due to Francis Andorful, George Lutterodt, and Jan Willem Foppen from the T-GroUP project for drilling observation well BH11, installing a diver, and permitting the use of the Dodowa groundwater hydrograph data. We thank Paula Cutillo and Shannon Mazzei from the National Park Service (NPS) in California (USA) for providing the barometric and groundwater pressure dataset for BLM-1. Some of the data used in this paper were collected with equipment provided by the Australian Federal Government financed *National Collaborative Research Infrastructure Strategy* (NCRIS). This project has received funding from the European Union's Horizon 2020 research and innovation programme under the Marie Skłodowska-Curie grant agreement No 835852. TCM was partly supported by an Australian Government Research Training Program (RTP) Scholarship.

References

Acworth, R. I., Halloran, L. J. S., Rau, G. C., Cuthbert, M. O., & Bernardi, T. L. (2016). An objective frequency domain method for quantifying confined aquifer

compressible storage using Earth and atmospheric tides. *Geophysical Research Letters*, *43*(22), 611–671. Retrieved from http://dx.doi.org/10.1002/2016GL071328 doi: 10.1002/2016GL071328

Acworth, R. I., Rau, G. C., Halloran, L. J. S., & Timms, W. A. (2017). Vertical groundwater storage properties and changes in confinement determined using hydraulic head response to atmospheric tides. *Water Resources Research*, *53*(4), 2983–2997. Retrieved from http://dx.doi.org/10.1002/2016WR020311 doi: 10.1002/2016WR020311

Acworth, R. I., Timms, W. A., Kelly, B. F., Mcgeeney, D. E., Ralph, T. J., Larkin, Z. T., & Rau, G. C. (2015). Late Cenozoic paleovalley fill sequence from the Southern Liverpool Plains, New South Wales—implications for groundwater resource evaluation. *Australian Journal of Earth Sciences*, *62*(6), 657–680. doi: 10.1080/08120099.2015.1086815

Agnew, D. C. (2010). Earth Tides. *Geodesy: Treatise on Geophysics*, 163.

Allègre, V., Brodsky, E. E., Xue, L., Nale, S. M., Parker, B. L., & Cherry, J. A. (2016, 4). Using earth-tide induced water pressure changes to measure in situ permeability: A comparison with long-term pumping tests. *Water Resources Research*, *52*(4), 3113–3126. Retrieved from http://doi.wiley.com/10.1002/2015WR017346 doi: 10.1002/2015WR017346

Attoh, K., Dallmeyer, R. D., & Affaton, P. (1997). Chronology of nappe assembly in the Pan-African Dahomeyide orogen, West Africa: evidence from 40Ar39Ar mineral ages. *Precambrian Research*, *82*(1), 153–171. Retrieved from http://www.sciencedirect.com/science/article/pii/S0301926896000319 doi: https://doi.org/10.1016/S0301-9268(96)00031-9

Barr, A. G., van der Kamp, G., Schmidt, R., & Black, T. A. (2000). Monitoring the moisture balance of a boreal aspen forest using a deep groundwater piezometer. *Agricultural and Forest Meteorology*, *102*(1), 13–24.

Beavan, J., Evans, K., Mousa, S., & Simpson, D. (1991, 7). Estimating aquifer parameters from analysis of forced fluctuations in well level: An example from the Nubian Formation near Aswan, Egypt: 2. Poroelastic properties. *Journal of Geophysical Research: Solid Earth*, *96*(B7), 12139–12160. Retrieved from https://doi.org/10.1029/91JB00956 doi: 10.1029/91JB00956

Bertuzzi, R. (2014). Sydney sandstone and shale parameters for tunnel design. *Aus-*

tralian Geomechanics Journal, *49*(1), 1–39.

Birch, F. (1996). Compressibility, elastic constants. In *Handbook of physical constants* (Vol. 97, pp. 97–174). New York: Geological Society of America.

Bouzalakos, S., Crane, R. A., McGeeney, D., & Timms, W. A. (2016). Stress-dependent hydraulic properties of clayey-silt aquitards in eastern Australia. *Acta Geotechnica*, *11*(5), 969–986.

Bower, D. R. (1983, 6). Bedrock fracture parameters from the interpretation of well tides. *Journal of Geophysical Research: Solid Earth*, *88*(B6), 5025–5035. Retrieved from `https://doi.org/10.1029/JB088iB06p05025` doi: 10.1029/JB088iB06p05025

Bowles, L. E. (1996). *Foundation analysis and design*. McGraw-hill.

Bredehoeft, J. D. (1967, 6). Response of well-aquifer systems to Earth tides. *Journal of Geophysical Research*, *72*(12), 3075–3087. Retrieved from `http://doi.wiley.com/10.1029/JZ072i012p03075` doi: 10.1029/JZ072i012p03075

Burbey, T. J. (2010). Fracture characterization using earth tide analysis. *Journal of Hydrology*, *380*(3), 237 - 246. Retrieved from `http://www.sciencedirect.com/science/article/pii/S0022169409007069` doi: https://doi.org/10.1016/j.jhydrol.2009.10.037

Burbey, T. J., Hisz, D., Murdoch, L. C., & Zhang, M. (2012, 1). Quantifying fractured crystalline-rock properties using well tests, earth tides and barometric effects. *Journal of Hydrology*, *414*, 317–328. Retrieved from `http://linkinghub.elsevier.com/retrieve/pii/S002216941100789X` doi: 10.1016/j.jhydrol.2011.11.013

Clark, W. E. (1967). Computing the barometric efficiency of a well. *Journal of the Hydraulics Division*, *93*(4), 93–98. Retrieved from `http://cedb.asce.org/CEDBsearch/record.jsp?dockey=0014622`

Colwell, M., & Frith, R. (2006). Why Uniaxial Compressive Strength and Young's Modulus Are Commonly Poor Indicators of Roadway Roof Stability-Except in the Tailgate. In *Coal 2006: Coal operators' conference, university of wollongong & the australasian institute of mining and metallurgy, 2006, 28-43.*

Condon, K. J., Sone, H., Wang, H. F., Ajo-Franklin, J., Baumgartner, T., Beckers, K., ... CollabTeam, E. G. S. (2020). Low Static Shear Modulus Along Foliation and Its Influence on the Elastic and Strength Anisotropy of Poorman

Schist Rocks, Homestake Mine, South Dakota. *Rock Mechanics and Rock Engineering*, *53*(11), 5257–5281. Retrieved from https://doi.org/10.1007/s00603-020-02182-4 doi: 10.1007/s00603-020-02182-4

Cundall, P. A., Pierce, M. E., & Mas Ivars, D. (2008). *Quantifying the Size Effect of Rock Mass Strength.* Perth: Australian Centre for Geomechanics PP - Perth. Retrieved from https://papers.acg.uwa.edu.au/p/808_31_Cundall/

Cutillo, P. A., & Bredehoeft, J. D. (2011, 7). Estimating Aquifer Properties from the Water Level Response to Earth Tides. *Ground Water*, *49*(4), 600–610. Retrieved from http://doi.wiley.com/10.1111/j.1745-6584.2010.00778.x doi: 10.1111/j.1745-6584.2010.00778.x

De Araujo, M. A. R., Campos, W., & Moreno, R. Z. (2012). *Filtering of Tide Effects in Formation Evaluation Data.* Mexico City, Mexico: Society of Petroleum Engineers. Retrieved from https://doi.org/10.2118/153566-MS doi: 10.2118/153566-MS

Foppen, J. W., Lutterodt, G., Rau, G. C., & Minkah, O. (2020). Groundwater flow system analysis in the regolith of Dodowa on the Accra Plains, Ghana. *Journal of Hydrology: Regional Studies*, *28*, 100663. Retrieved from http://www.sciencedirect.com/science/article/pii/S2214581819300552 doi: https://doi.org/10.1016/j.ejrh.2020.100663

Fuentes-Arreazola, M., Ramírez-Hernández, J., & Vázquez-González, R. (2018, 5). Hydrogeological Properties Estimation from Groundwater Level Natural Fluctuations Analysis as a Low-Cost Tool for the Mexicali Valley Aquifer. *Water*, *10*(5), 586. Retrieved from http://www.mdpi.com/2073-4441/10/5/586 doi: 10.3390/w10050586

Gao, X., Sato, K., & Horne, R. N. (2020, 6). General Solution for Tidal Behavior in Confined and Semiconfined Aquifers Considering Skin and Wellbore Storage Effects. *Water Resources Research*, *56*(6), e2020WR027195. Retrieved from https://doi.org/10.1029/2020WR027195 doi: 10.1029/2020WR027195

Gercek, H. (2007). Poisson's ratio values for rocks. *International Journal of Rock Mechanics and Mining Sciences*, *44*(1), 1–13. Retrieved from http://www.sciencedirect.com/science/article/pii/S136516090600075X doi: https://doi.org/10.1016/j.ijrmms.2006.04.011

Gonthier, G. (2003). *A Graphical Method for Estimation of Barometric Efficiency*

from Continuous Data - Concepts and Application to a Site in the Piedmont, Air Force Plant 6, Marietta, Georgia (Tech. Rep.). US Geological Survey. Retrieved from https://pubs.er.usgs.gov/publication/sir20075111 doi: 10.3133/sir20075111

Green, D. H., & Wang, H. F. (1990, 7). Specific storage as a poroelastic coefficient. *Water Resources Research*, *26*(7), 1631–1637. Retrieved from https://doi.org/10.1029/WR026i007p01631 doi: 10.1029/WR026i007p01631

Handin, J., Hager Jr, R. V., Friedman, M., & Feather, J. N. (1963). Experimental deformation of sedimentary rocks under confining pressure: pore pressure tests. *Aapg Bulletin*, *47*(5), 717–755.

Hanson, J. M., & Owen, L. B. (1982, 4). Fracture orientation analysis by the solid earth tidal strain method. In *Proceedings - spe annual technical conference and exhibition* (Vol. 1982-Septe, p. 18). New Orleans, Louisiana: Society of Petroleum Engineers. Retrieved from http://www.onepetro.org/doi/10.2118/11070-MShttps://doi.org/10.2118/11070-MS doi: 10.2118/11070-MS

Hoek, E., & Diederichs, M. S. (2006). Empirical estimation of rock mass modulus. *International Journal of Rock Mechanics and Mining Sciences*, *43*(2), 203–215. Retrieved from http://www.sciencedirect.com/science/article/pii/S1365160905000948 doi: https://doi.org/10.1016/j.ijrmms.2005.06.005

Homand-Etienne, F., & Houpert, R. (1989). Thermally induced microcracking in granites: characterization and analysis. *International Journal of Rock Mechanics and Mining Sciences & Geomechanics Abstracts*, *26*(2), 125–134. Retrieved from http://www.sciencedirect.com/science/article/pii/0148906289900016 doi: https://doi.org/10.1016/0148-9062(89)90001-6

Hsieh, P. A., Bredehoeft, J. D., & Farr, J. M. (1987, 10). Determination of aquifer transmissivity from Earth tide analysis. *Water Resources Research*, *23*(10), 1824–1832. Retrieved from http://doi.wiley.com/10.1029/WR023i010p01824 doi: 10.1029/WR023i010p01824

Hsieh, P. A., Bredehoeft, J. D., & Rojstaczer, S. A. (1988, 3). Response of well aquifer systems to Earth tides: Problem revisited. *Water Resources Research*, *24*(3), 468–472. Retrieved from http://dx.doi.org/10.1029/WR024i003p00468http://doi.wiley.com/10.1029/WR024i003p00468 doi:

10.1029/WR024i003p00468

Impax. (2019). *Impax Drilling correspondance and drill reports: Thirlmere 1 and 2* (Tech. Rep.).

Jacob, C. E. (1939). Fluctuations in artesian pressure produced by passing railroad-trains as shown in a well on Long Island, New York. *Transactions, American Geophysical Union*, *20*(4), 666. Retrieved from `http://doi.wiley.com/10.1029/TR020i004p00666` doi: 10.1029/TR020i004p00666

Jacob, C. E. (1940). On the flow of water in an elastic artesian aquifer. *Eos, Transactions American Geophysical Union*, *21*(2), 574–586.

Ji, S., Li, L., Motra, H. B., Wuttke, F., Sun, S., Michibayashi, K., & Salisbury, M. H. (2018, 2). Poisson's Ratio and Auxetic Properties of Natural Rocks. *Journal of Geophysical Research: Solid Earth*, *123*(2), 1161–1185. Retrieved from `https://doi.org/10.1002/2017JB014606` doi: 10.1002/2017JB014606

Johnson, P. A., & Rasolofosaon, P. N. J. (1996, 2). Nonlinear elasticity and stress-induced anisotropy in rock. *Journal of Geophysical Research: Solid Earth*, *101*(B2), 3113–3124. Retrieved from `https://doi.org/10.1029/95JB02880` doi: 10.1029/95JB02880

Khan, A. S., Xiang, Y., & Huang, S. (1991). Behavior of Berea sandstone under confining pressure part I: Yield and failure surfaces, and nonlinear elastic response. *International Journal of Plasticity*, *7*(6), 607–624. Retrieved from `http://www.sciencedirect.com/science/article/pii/0749641991900462` doi: https://doi.org/10.1016/0749-6419(91)90046-2

Kümpel, H.-J. (1997). Tides in water saturated rock BT - Tidal Phenomena. In H. Wilhelm, W. Zürn, & H.-G. Wenzel (Eds.), (pp. 277–291). Berlin, Heidelberg: Springer Berlin Heidelberg. Retrieved from `https://doi.org/10.1007/BFb0011467` doi: 10.1007/BFb0011467

Lakes, R. (1991). Deformation mechanisms in negative Poisson's ratio materials: structural aspects. *Journal of Materials Science*, *26*(9), 2287–2292. Retrieved from `https://doi.org/10.1007/BF01130170` doi: 10.1007/BF01130170

Lakes, R. S., & Witt, R. (2002). Making and characterizing negative Poisson's ratio materials. *International Journal of Mechanical Engineering Education*, *30*(1), 50–58.

Leriche, A. (2017). *Stress estimation from borehole scans for prediction of exca-*

vation overbreak in brittle rock. (Unpublished doctoral dissertation). Kingston, Ontario, Canada: Queen's University.

Masoumi, H., Douglas, K. J., & Russell, A. R. (2016, 1). A Bounding Surface Plasticity Model for Intact Rock Exhibiting Size-Dependent Behaviour. *Rock Mechanics and Rock Engineering*, *49*(1), 47–62. Retrieved from http://link.springer.com/10.1007/s00603-015-0744-8 doi: 10.1007/s00603-015-0744-8

McMillan, T. C., Rau, G. C., Timms, W. A., & Andersen, M. S. (2019, 6). Utilizing the Impact of Earth and Atmospheric Tides on Groundwater Systems: A Review Reveals the Future Potential. *Reviews of Geophysics*, *57*(2), 281–315. Retrieved from https://onlinelibrary.wiley.com/doi/abs/10.1029/2018RG000630 doi: 10.1029/2018RG000630

Merritt, M. L. (2004). *Estimating hydraulic properties of the Floridan Aquifer System by analysis of earth-tide, ocean-tide, and barometric effects, Collier and Hendry Counties, Florida* (Tech. Rep.). Retrieved from https://pubs.er.usgs.gov/publication/wri034267 doi: 10.3133/wri034267

Miall, A. D., & Jones, B. G. (2003). Fluvial architecture of the Hawkesbury sandstone (Triassic), near Sydney, Australia. *Journal of Sedimentary Research*, *4*(73), 531–545.

Narasimhan, T. N., Kanehiro, B. Y., & Witherspoon, P. A. (1984, 3). Interpretation of Earth tide response of three deep, confined aquifers. *Journal of Geophysical Research: Solid Earth*, *89*(B3), 1913–1924. Retrieved from http://doi.wiley.com/10.1029/JB089iB03p01913 doi: 10.1029/JB089iB03p01913

Parent, T., Domede, N., Sellier, A., & Mouatt, L. (2015). Mechanical characterization of limestone from sound velocity measurement.

Pimienta, L., Fortin, J., & Guéguen, Y. (2016, 3). Effect of fluids and frequencies on Poisson's ratio of sandstone samples. *Geophysics*, *81*(2), D183-D195. Retrieved from https://doi.org/10.1190/geo2015-0310.1 doi: 10.1190/geo2015-0310.1

Rasmussen, T. C., & Crawford, L. A. (1997, 5). Identifying and Removing Barometric Pressure Effects in Confined and Unconfined Aquifers. *Ground Water*, *35*(3), 502–511. Retrieved from http://doi.wiley.com/10.1111/j.1745-6584.1997.tb00111.x doi: 10.1111/j.1745-6584.1997.tb00111.x

Rau, G. C. (2018). *PyGTide: A Python module and wrapper for ETERNA PREDICT to compute synthetic model tides on Earth.* Zenodo. Retrieved from https://doi.org/10.5281/zenodo.1346260 doi: 10.5281/zenodo.1346260

Rau, G. C., Acworth, R. I., Halloran, L. J. S., Timms, W. A., & Cuthbert, M. O. (2018, 8). Quantifying Compressible Groundwater Storage by Combining Cross-Hole Seismic Surveys and Head Response to Atmospheric Tides. *Journal of Geophysical Research: Earth Surface*, *123*(8), 1910–1930. Retrieved from https://doi.org/10.1029/2018JF004660http://doi.wiley.com/10.1029/2018JF004660 doi: 10.1029/2018JF004660

Rau, G. C., Cuthbert, M. O., Acworth, I. R., & Blum, P. (2020). Technical Note: Disentangling the groundwater response to Earth and atmospheric tides to improve subsurface characterisation. *Hydrology and Earth System Science Discussion*. doi: 10.5194/hess-2020-256

Rau, G. C., Post, V. E. A., Shanafield, M., Krekeler, T., Banks, E. W., & Blum, P. (2019, 9). Error in hydraulic head and gradient time-series measurements: a quantitative appraisal. *Hydrology and Earth System Sciences*, *23*(9), 3603–3629. Retrieved from https://www.hydrol-earth-syst-sci-discuss.net/hess-2019-182/https://www.hydrol-earth-syst-sci.net/23/3603/2019/ doi: 10.5194/hess-23-3603-2019

Richardson, N. D., Williams, K. L., Briggs, K. B., & Thorsos, E. I. (2002). Dynamic measurement of sediment grain compressibility at atmospheric pressure: acoustic applications. *IEEE Journal of Oceanic Engineering*, *27*(3), 593–601. doi: 10.1109/JOE.2002.1040941

Ritzi, R. W., Sorooshian, S., & Hsieh, P. A. (1991, 5). The estimation of fluid flow properties from the response of water levels in wells to the combined atmospheric and Earth tide forces. *Water Resources Research*, *27*(5), 883–893. Retrieved from http://doi.wiley.com/10.1029/91WR00070 doi: 10.1029/91WR00070

Roeloffs, E. (1996). Poroelastic Techniques in the Study of Earthquake-Related Hydrologic Phenomena. In *Advances in geophysics* (Vol. 38, pp. 135–195). Retrieved from https://linkinghub.elsevier.com/retrieve/pii/S0065268708602708 doi: 10.1016/S0065-2687(08)60270-8

Roeloffs, E. A., Burford, S. S., Riley, F. S., & Records, A. W. (1989). Hydro-

logic effects on water level changes associated with episodic fault creep near Parkfield, California. *Journal of Geophysical Research*, *94*(B9), 12387. Retrieved from http://doi.wiley.com/10.1029/JB094iB09p12387 doi: 10.1029/jb094ib09p12387

Rojstaczer, S. (1988). Determination of fluid flow properties from the response of water levels in wells to atmospheric loading. *Water Resources Research*, *24*(11), 1927–1938. doi: 10.1029/WR024i011p01927

Rojstaczer, S., & Agnew, D. C. (1989). The influence of formation material properties on the response of water levels in wells to Earth tides and atmospheric loading. *Journal of Geophysical Research*, *94*(B9), 12403. Retrieved from http://doi.wiley.com/10.1029/JB094iB09p12403 doi: 10.1029/JB094iB09p12403

Rojstaczer, S., & Riley, F. S. (1990). Response of the water level in a well to Earth tides and atmospheric loading under unconfined conditions. *Water Resources Research*, *26*(8), 1803–1817. doi: 10.1029/WR026i008p01803

Ross, J. B. (2014). Groundwater resource potential of the Triassic Sandstones of the Southern Sydney Basin: an improved understanding. *Australian Journal of Earth Sciences*, *61*(3), 463–474. Retrieved from http://dx.doi.org/10.1080/08120099.2014.910548 doi: 10.1080/08120099.2014.910548

Russell, G. (2012). *Thirlmere Lakes drilling report* (Tech. Rep.). Sydney: NSW Office of Water.

SCA. (2005). *Metropolitan Water Plan. Priority Groundwater Investigations for Emergency Drought Relief. Area 2: Upper Nepean Catchment.* (Tech. Rep.).

SCA. (2006). *Upper Nepean Groundwater Pilot Studies - Pumping Test Interpretation and Data Logger Installation* (Tech. Rep.).

Schulze, K. C., Kümpel, H.-J., & Huenges, E. (2000). In-Situ Petrohydraulic Parameters from Tidal and Barometric Analysis of Fluid Level Variations in Deep Wells: Some Results From KTB BT - Hydrogeology of Crystalline Rocks. In I. Stober & K. Bucher (Eds.), (pp. 79–104). Dordrecht: Springer Netherlands. Retrieved from https://doi.org/10.1007/978-94-017-1816-5_4 doi: 10.1007/978-94-017-1816-5{_}4

Sheriff, R. E. (2002). *Encyclopedic dictionary of applied geophysics.* Society of exploration geophysicists.

Shi, Z., & Wang, G. (2016, 11). Aquifers switched from confined to semiconfined by earthquakes. *Geophysical Research Letters*, *43*(21), 111–166. Retrieved from https://doi.org/10.1002/2016GL070937 doi: 10.1002/2016GL070937

Timms, W. A., & Acworth, R. I. (2005, 10). Propagation of pressure change through thick clay sequences: an example from Liverpool Plains, NSW, Australia. *Hydrogeology Journal*, *13*(5-6), 858–870. Retrieved from http://link.springer.com/10.1007/s10040-005-0436-7 doi: 10.1007/s10040-005-0436-7

Timms, W. A., Acworth, R. I., Crane, R. A., Arns, C. H., Arns, J., McGeeney, D. E., ... Cuthbert, M. O. (2018). The influence of syndepositional macropores on the hydraulic integrity of thick alluvial clay aquitards. *Water Resources Research*, *54*(4), 3122–3138.

Turnadge, C., Crosbie, R. S., Barron, O., & Rau, G. C. (2019, 11). Comparing Methods of Barometric Efficiency Characterization for Specific Storage Estimation. *Groundwater*, *57*(6), 844–859. Retrieved from https://onlinelibrary.wiley.com/doi/abs/10.1111/gwat.12923 doi: 10.1111/gwat.12923

Tutuncu, A. N., Podio, A. L., Gregory, A. R., & Sharma, M. M. (1998, 2). Nonlinear viscoelastic behavior of sedimentary rocks, Part I: Effect of frequency and strain amplitude. *Geophysics*, *63*(1), 184–194. Retrieved from https://doi.org/10.1190/1.1444311 doi: 10.1190/1.1444311

Van Camp, M., & Vauterin, P. (2005, 6). Tsoft: graphical and interactive software for the analysis of time series and Earth tides. *Computers & Geosciences*, *31*(5), 631–640. Retrieved from http://linkinghub.elsevier.com/retrieve/pii/S0098300404002456 doi: 10.1016/j.cageo.2004.11.015

van der Kamp, G., & Gale, J. E. (1983). Theory of earth tide and barometric effects in porous formations with compressible grains. *Water Resources Research*, *19*(2), 538–544. Retrieved from http://dx.doi.org/10.1029/WR019i002p00538 doi: 10.1029/WR019i002p00538

Villeneuve, M. C., Heap, M. J., Kushnir, A. R. L., Qin, T., Baud, P., Zhou, G., & Xu, T. (2018). Estimating in situ rock mass strength and elastic modulus of granite from the Soultz-sous-Forêts geothermal reservoir (France). *Geothermal Energy*, *6*(1), 11. Retrieved from https://doi.org/10.1186/s40517-018-0096-1 doi: 10.1186/s40517-018-0096-1

Wang, H. F. (1993). Quasi-static poroelastic parameters in rock and their geophysical applications. *pure and applied geophysics*, *141*(2), 269–286. Retrieved from https://doi.org/10.1007/BF00998332 doi: 10.1007/BF00998332

Wang, H. F. (2000). *Theory of Linear Poroelasticity with Applications to Geomechanics and Hydrogeology.* Princeton University Press. Retrieved from https://press.princeton.edu/titles/7006.html

Wang, K., & Davis, E. E. (1996). Theory for the propagation of tidally induced pore pressure variations in layered subseafloor formations. *Journal of Geophysical Research: Solid Earth*, *101*(B5), 11483–11495.

Wenzel, H.-G. (1996). Accuracy assessment for tidal potential catalogues. *Bulletin d'Informations des Marées Terrestres*, *124*, 9394–9416.

Xue, L., Brodsky, E. E., Erskine, J., Fulton, P. M., & Carter, R. (2016, 3). A permeability and compliance contrast measured hydrogeologically on the San Andreas Fault. *Geochemistry, Geophysics, Geosystems*, *17*(3), 858–871. Retrieved from https://doi.org/10.1002/2015GC006167 doi: 10.1002/2015GC006167

Zaitsev, V. Y., Radostin, A. V., Pasternak, E., & Dyskin, A. (2017). Extracting real-crack properties from non-linear elastic behaviour of rocks: abundance of cracks with dominating normal compliance and rocks with negative Poisson ratios. *Nonlinear Processes in Geophysics*, *24*(3), 543–551. Retrieved from https://npg.copernicus.org/articles/24/543/2017/ doi: 10.5194/npg-24-543-2017

Zhang, C., & Lu, N. (2018, 9). What Is the Range of Soil Water Density? Critical Reviews With a Unified Model. *Reviews of Geophysics*, *56*(3), 532–562. Retrieved from http://doi.wiley.com/10.1029/2018RG000597 doi: 10.1029/2018RG000597

Zhang, C., Mitra, R., Oh, J., & Hebblewhite, B. (2016). Analysis of Mining-induced Valley Closure Movements. *Rock Mechanics and Rock Engineering*, *49*(5), 1923–1941. doi: 10.1007/s00603-015-0880-1

Zhang, S., Shi, Z., & Wang, G. (2019). Comparison of aquifer parameters inferred from water level changes induced by slug test, earth tide and earthquake – A case study in the three Gorges area. *Journal of Hydrology*, *579*, 124169. Retrieved from http://www.sciencedirect.com/science/article/pii/

S0022169419309047 doi: https://doi.org/10.1016/j.jhydrol.2019.124169

Zhao, Z., Xu, H., Wang, J., Zhao, X., Cai, M., & Yang, Q. (2020). Auxetic behavior of Beishan granite after thermal treatment: A microcracking perspective. *Engineering Fracture Mechanics*, *231*, 107017. Retrieved from http://www.sciencedirect.com/science/article/pii/S0013794420301636 doi: https://doi.org/10.1016/j.engfracmech.2020.107017